HHS Public Access

Author manuscript

Nat Aging. Author manuscript; available in PMC 2022 February 01.

Published in final edited form as:

Nat Aging. 2021 August ; 1(8): 715–733. doi:10.1038/s43587-021-00086-8.

Multi-omic profiling of primary mouse neutrophils predicts a pattern of sex and age-related functional regulation

Ryan J. Lu[1,2], **Shalina Taylor**[3], **Kévin Contrepois**[4], **Minhoo Kim**[1], **Juan I. Bravo**[1,2], **Mathew Ellenberger**[4], **Nirmal K. Sampathkumar**[1,5], **Bérénice A. Benayoun**[1,6,7,8,§]

[1]Leonard Davis School of Gerontology, University of Southern California, Los Angeles, CA 90089, USA.

[2]Graduate program in the Biology of Aging, University of Southern California, Los Angeles, CA 90089, USA.

[3]Departments of Pediatrics and of Medicine, Stanford University School of Medicine, Stanford, CA 94305, USA.

[4]Department of Genetics, Stanford University, Stanford, CA 94305, USA.

[5]Present Address: UK-Dementia Research Institute, Institute of Psychiatry, Psychology and Neuroscience, Basic and Clinical Neuroscience Institute, Maurice Wohl Clinical Neuroscience Institute, King's College London, London, UK

[6]USC Norris Comprehensive Cancer Center, Epigenetics and Gene Regulation, Los Angeles, CA 90089, USA.

[7]Molecular and Computational Biology Department, USC Dornsife College of Letters, Arts and Sciences, Los Angeles, CA 90089.

[8]USC Stem Cell Initiative, Los Angeles, CA 90089, USA.

Abstract

Neutrophils are the most abundant human white blood cell and constitute a first line of defense in the innate immune response. Neutrophils are short-lived cells, and thus the impact of organismal aging on neutrophil biology, especially as a function of biological sex, remains poorly understood. Here, we describe a multi-omic resource of mouse primary bone marrow neutrophils from young and old female and male mice, at the transcriptomic, metabolomic and lipidomic levels. We identify widespread regulation of neutrophil 'omics' landscapes with organismal aging and biological sex. In addition, we leverage our resource to predict functional differences, including

[§]Corresponding Author. berenice.benayoun@usc.edu.

Author Contributions Statement

S.T. and B.A.B. designed the study. R.J.L., S.T., M.K., N.K. and B.A.B. isolated and/or processed neutrophil samples. R.J.L. and B.A.B. performed flow cytometry experiments to characterize neutrophils' phenotypes. K.C. experimentally processed samples for metabolomic and lipidomic profiling and pre-processed the resulting data. M.K. performed neutrophil protein extraction and Western blotting experiments. K.C. and M.E. performed the manual validation/identification of significant metabolites from the untargeted metabolomics data. R.L. and B.A.B. conducted the "sepsis-like" experiment. J.I.B performed the HEMAVET quantifications of cell types on bone marrow cell suspensions. B.A.B. performed data analyses. B.A.B wrote the manuscript with input from all the authors. All authors edited and commented on the manuscript.

Competing Interests Statement

The authors declare no competing interests.

changes in neutrophil responses to activation signals. To date, this dataset represents the largest multi-omics resource for neutrophils across sex and ages. This resource identifies neutrophil characteristics which could be targeted to improve immune responses as a function of sex and/or age.

Introduction

Neutrophils are the most abundant cells in human blood, representing 50–70% of leukocytes[1]. These cells are continually produced in the bone marrow and released into circulation[2, 3]. Neutrophils are short-lived, with estimated cellular lifespans of ~10–18 hours once released in the bloodstream[4, 5], although they can survive longer[4, 6]. Throughout their cellular lifespan, neutrophils undergo “neutrophil aging”, a process distinct from organismal aging[3, 7]. Neutrophils perform many key functions, including production of antimicrobial granules and of “Neutrophil Extracellular Traps” [NETs][3, 8]. Although neutrophils are essential against infections as the “first line of defense”, their aberrant activation can also aggravate inflammatory disease[2, 3]. Indeed, emerging evidence suggests that neutrophils play important roles in chronic inflammation[9].

Organismal aging in mammals is characterized by systematic immune dysfunction and chronic inflammation, a phenomenon dubbed “inflamm-aging”[10], which may be partially mediated by dysfunction of innate immune cells[11]. Indeed, emerging evidence suggests that neutrophils from aged organisms are dysfunctional[12, 13, 14, 15, 16]. Observed age-related dysfunctions in neutrophils include decreased NETosis in TNFα-primed conditions[13, 14], reduced chemotaxis to sites of inflammation[15] and secretion of intracellular granule proteases[15, 17]. Although gene expression changes throughout lifespan have been reported across many cell types[18, 19], how organismal aging (rather than “daily” cell aging) affects neutrophil landscapes remains largely unknown.

Females and males present with many biological differences, which may underlie lifelong health disparities between sexes[20] and could result from differential “omic” regulation[21, 22]. Although transcriptional differences between young female and male murine neutrophils have been profiled by ImmGen[22], how these differences interplay with organismal aging, and whether they are accompanied by other phenotypical differences remains largely unknown. Accumulated studies suggest that aspects of neutrophil biology are sex-dimorphic, *e.g.* inflammatory mediators production[9], or functional modulation by testosterone[23]. However, the pathways underlying sex-dimorphism in neutrophils, as well as the extent of sex-dimorphism, are still unclear.

To gain insights into how neutrophils are regulated as a function of age and sex, we generated a “multi-omic” resource covering transcriptome, metabolome and lipidome profiling of primary bone marrow mouse neutrophils. We identified widespread age-related and sex-dimorphic “omic” regulation, including transcriptional regulation of chromatin-related pathways. Using ATAC-seq, we showed that remodeling of chromatin-related pathways was associated with overall differences in the chromatin architecture of neutrophils from young *vs.* old and female *vs.* male mice. Consistently, we observed age- and sex-linked differences in NETosis inducibility. Machine-learning showed that specific

factors could predict age-related and sex-dimorphic gene regulation in neutrophils. Finally, we leveraged our resource and predicted sex-differences in serum levels of neutrophil elastase in control and sepsis-like conditions.

Results

Multi-omics of bone marrow neutrophils with age and sex

To understand how neutrophils are regulated as a function of age and sex, we obtained primary bone marrow neutrophils from young (4–5 months) and old (20–21 months) C57BL/6Nia female and male mice (Figure 1a). Primary neutrophils were isolated from bone marrow using magnetic-activated cell sorting [MACS], and profiling was then performed on purified neutrophils: (i) transcriptome profiling by RNA-sequencing [RNA-seq], (ii) metabolomic profiling by untargeted liquid chromatography coupled with mass spectrometry [LC-MS], and (iii) lipidomic profiling by targeted MS (Figure 1a).

As a first-level analysis to evaluate the similarity of our datasets, we utilized multidimensional scaling [MDS]. MDS analysis for RNA-seq, metabolomics and lipidomics datasets showed clear separation of samples by animal sex, regardless of age (Figure 1b–d). In contrast, although young and old samples separated within each sex, global separation by age regardless of sex was not clearly observed for each omics (Figure 1 b–d). To better understand the nature of differences between neutrophils from young *vs.* old [with sex as a covariate], and female *vs.* male animals [with age as a covariate], we identified transcriptional, metabolic and lipidomic features with significant age- or sex-related regulation at a False Discovery Rate [FDR] < 5% using multivariate linear modeling (Figure 1e–g and Extended Data Figure 1a–f; Supplementary Table S1A–F). We quality-checked our dataset for appropriate expression of sex-specific genes (Extended Data Figure 1b,c). Finally, we confirmed differential gene expression trends between groups using a small replicate RNA-seq cohort (Extended Data Figure 2a,b), and comparing our data with published datasets from female *vs.* males mouse spleen neutrophils[22] and human blood neutrophils[24] (Extended Data Figure 2a). Thus, our analyses suggest that observed transcriptional differences with respect to organismal age and sex in neutrophils are robust.

Consistent with MDS, we identified genes, metabolic features and lipids with significant differential regulation with respect to sex (FDR < 5%; Figure 1e–g and Extended Data Figure 1a–d; Supplementary Table S1B,D,E). Differentially expressed genes with respect to sex were located throughout the genome, suggesting that sex-dimorphic gene expression was not just a byproduct of genomic location (Extended Data Figure 1a,e). Importantly, we observed no biases in the purity of MACS-purified neutrophils across groups (Extended Data Figure 3a–b), and no difference in neutrophil abundance in bone-marrow (Extended Data Figure 3c) across groups. Thus, sex-dimorphic and age-related “omic” phenotypes are unlikely to result from a systematic purification bias between groups.

Although aging led to clear changes in neutrophil gene expression profiles (Extended Data Figure 1a,f; Supplementary Table S1), few to no metabolomic and lipidomic changes were observed (Extended Data Figure 1a; Supplementary Table S1C,F). This is consistent with overall poorer age-related separation observed for metabolomics and lipidomics (Figure

1c–d). Higher biological variability in metabolites and lipids might explain the lack of changes with age. Alternatively, it is possible that the paucity of age-related metabolic and lipidomic differences may stem from biological specificities of neutrophils (*e.g.* short cellular lifespan). When female and male neutrophils were analyzed separately, we found that the transcriptional impact of aging on neutrophils correlated strongly between sexes (Spearman Rho = 0.593 and p ~ 0 in significance of correlation test; Extended Data Figure 1g). Thus, although neutrophils show clear sex differences throughout life, the trajectories of neutrophils with aging are highly similar regardless of sex. To note, we observed a greater number of transcriptional changes with organismal age in male *vs.* female neutrophils (Extended Data Figure 1h), suggesting that male neutrophils are more susceptible to aging. Together, our results indicate that neutrophils are highly sex-dimorphic at the molecular level, and that these sex differences persist (or may be amplified) with organismal aging.

Finally, since bone marrow neutrophils can be heterogenous, we evaluated the composition of MACS-purified neutrophils across groups (Extended Data Figure 4a–d; Supplementary Table S2A,B). We leveraged flow cytometry markers to estimate the proportions of neutrophil progenitors (*i.e.* pre- and pro-neutrophils), immature *vs.* mature neutrophils, and fresh *vs.* "aged" neutrophils in our population. Neutrophil progenitors were extremely rare among MACS-purified cells (*i.e.* pre- and pro-neutrophils represent < 0.5% of cells; Extended Data Figure 4a; Supplementary Table S2A), and are unlikely to drive large "omic" differences. Importantly, we did not observe significant differences in the presence of mature *vs.* immature neutrophils across groups (Extended Data Figure 4a,c; Supplementary Table S2). Finally, we observed a significant trend for the increased presence of senescent/aged neutrophils ($CD62L^{-}$) among the mature neutrophils (Extended Data Figure 4a,d; Supplementary Table S2A). Our observation is consistent with a previous report of accumulation of senescent/aged neutrophils in old mice due to decreased clearance by efferocytosis[25]. Based on previous studies of senescent/aged neutrophils, changes in the relative proportion of "fresh" *vs.* "aged" neutrophils among bone marrow neutrophils may have functional impacts on inflammation, chemotaxis, and NETosis[26, 27].

Age-associated changes in chromatin pathways in neutrophils

We first focused on the impact of organismal aging on neutrophils using pathway enrichment analysis (Figure 2a–c and Extended Data Figure 5a–b; Supplementary Table S3). To note, we only analyzed age-related functional remodeling at the transcriptomic level, since metabolomics and lipidomics showed little changes with aging (Extended Data Figure 1a).

We assessed the coordination of age-related changes by performing a network analysis (Figure 2a). The network was constructed using age-regulated genes and protein-protein interaction [PPI] information from IMEx/InnateDB. Our analysis revealed that significantly age-regulated genes form a clearly interconnected network (Figure 2a). The strong interconnection of age-related genes is consistent with the notion that coordinated shifts occur in neutrophils with organismal aging, rather than stochastic changes, and suggests that these genes are co-regulated or are involved in common processes.

We then asked which pathways were regulated with aging (Figure 2b and Extended Data Figure 5a,b; Supplementary Table S3). Immune-related pathways were significantly upregulated according to Gene Set Enrichment Analysis [GSEA] (Figure 2b and Extended Data Figure 5a,b; Supplementary Table S3A–C) and Ingenuity Pathway Analysis [IPA] (Supplemental Table S3E). This suggests that neutrophil-associated immunity in older animals could have different characteristics, consistent with age-related immune dysfunction[10].

Intriguingly, the top downregulated pathways with organismal aging were overwhelmingly related to chromatin and cell cycle (Figure 2b and Extended Data Figure 5a,b; Supplementary Table S3A–C,E). Specifically, 18 histone-encoding genes were significantly downregulated with aging (Supplemental Table S1A). Importantly, we did not observe significant differences in the cell-cycle phase distribution of MACS-isolated neutrophils across groups (Extended Data Figure 6a,b), suggesting that differential expression of cell-cycle pathways is not a byproduct of differential proliferation.

Changes in the regulation of chromatin components are especially relevant to neutrophil biology. Indeed, neutrophils have a unique chromatin organization[28], with increased chromatin compaction or “supercontraction”[29]. In addition, neutrophils can extrude their chromatin to produce NETs in response to pathogens[30]. The extrusion of chromatin directly participates in pathogen killing, notably thanks to antimicrobial properties of histones[31]. Chromatin relaxation can also be potentiated by nuclear-translocated granule-derived proteases (*e.g.* Elane), ultimately helping bacterial killing[32]. Finally, although neutrophils are post-mitotic, cell-cycle genes can control NET production[33]. Thus, our analysis suggests that neutrophils may experience changes in chromatin organization with organismal aging, a feature that may impact their ability to respond to infection.

We also observed that several autophagy-related pathways were upregulated in old neutrophils (Figure 2b; Supplementary Table S3B,C,E). This is consistent with loss of proteostasis being a “hallmark of aging”[34]. Control of autophagy is critical for neutrophil differentiation[35], regulation of NET formation[36] and of degranulation[37].

To identify candidate upstream regulators, we investigated whether target genes of specific transcription factors [TFs] were differentially regulated with aging (Figure 2c; Supplementary Table S3D). We obtained lists of TF target genes derived from ChEA, JASPAR or GEO through the Harmonizome (see methods). Importantly, we restricted our testing to TFs with detectable expression in neutrophils according to RNA-seq. To note, the GEO “TF” set from Harmonizome includes several non-TF regulators (*e.g.* chromatin-remodeling enzymes, signaling receptors), which are referred to hereafter as TFs for simplicity. Consistent with functional pathway enrichments, we observed significant age-related downregulation of E2f7 targets, which are known to regulate cycle-related expression[38, 39] (Figure 2c). Although E2f7 has not been studied in neutrophils, it is highly expressed in committed progenitors[40]. Targets of Foxo1 were also significantly downregulated with aging in neutrophils (Figure 2c). Foxo TFs are the primary targets of the aging-regulating insulin/insulin-like growth factor 1 signaling[41], and Foxo1 regulates neutrophil-mediated bacterial immunity[42]. Finally, known targets of Padi4 were significantly

downregulated with aging (Figure 2c). Padi4 is a peptidylarginine deaminase, catalyzing histone citrullination, which plays a key role in NETosis *in vivo*[43, 44]. Transcript levels of *Padi4* were significantly upregulated with aging (FDR = 6.9×10^{-3}; Extended Data Figure 5c; Supplementary Table S1B). Protein levels of Padi4 were also significantly upregulated with aging regardless of sex ($p = 8.5\times10^{-3}$; Extended Data Figure 5d,e). This is consistent with reports of histone citrullination associating to transcriptional repression[45, 46, 47], although the directionality of regulation may depend on cofactors and cell types[48]. Together, our functional pathway analysis suggests that major aspects of chromatin metabolism are shifting in aging bone marrow neutrophils.

Sex-dimorphism in chromatin pathways in neutrophils

We next analyzed the functional impact of neutrophil sex-dimorphism at the transcriptomic, metabolomic and lipidomic levels (Figure 3a–f and Extended Data Figure 7a–c; Supplementary Table S4). We first assessed the interconnection of sex-dimorphic genes by constructing putative PPI networks for female *vs.* male-biased gene expression (Figure 3a,b). Sex-biased gene programs showed clear interconnection, suggesting coherent differences with likely functional impact (Figure 3a,b). The top connected node in the female-biased gene network, *Iqcb1*, encodes a primary cilia component and has been linked to severe kidney disease[49] (Figure 3a). Interestingly, *Irf8* was the top connected node in the male-biased gene network (Figure 3b). Although not specifically studied in neutrophils, Irf8 is an interferon signaling-related TF that regulates myeloid fate determination, usually suppressing neutrophil differentiation[50, 51]. In this context, Irf8 is likely to accomplish functions unrelated to myeloid differentiation (*e.g.* cytokine production)[52], since no significant changes in relative bone marrow neutrophil abundances were observed (Extended Data Figure 3c).

Next, we asked which pathways were regulated in a sex-dimorphic fashion in neutrophils (Figure 3c and Extended Data Figure 7a,b;` Supplementary Table S4). Functional enrichment analysis revealed that significant female-biased pathways encompassed extra-cellular matrix [ECM] and cell surface-related pathways (Figure 3c and Extended Data Figure 7a,b; Supplementary Table S4A–D). Indeed, collagen-encoding genes *Col1a1* and *Col1a2* were expressed at higher levels in female neutrophils (Supplementary Table S1B). Collagen production, usually from fibroblasts, is a key event in fibrosis[53], and neutrophils play an important role in the development of fibrotic lesions[54]. Alternatively, differential expression of cell surface-related genes may also impact the ability of neutrophils to migrate through endothelial barriers[55]. Interestingly, autophagy-related gene sets were female-biased in our dataset (Supplementary Table S4A,C,E). As mentioned above, autophagy control is critical for neutrophil biology[35, 36], including neutrophil degranulation[37].

Intriguingly, chromatin- and cell cycle-related pathways were overwhelmingly biased for higher expression in male neutrophils (Figure 3c; Extended Data Figure 7a,b; Supplementary Table S4A–C). Consistently, 21 histone-encoding genes showed significant male-biased expression (Supplementary Table S1B). The sex-dimorphic regulation of chromatin-related pathways suggests that sex may lead to differences in neutrophil chromatin metabolism.

We next investigated whether sex-dimorphic expression was correlated with predicted activity of TFs in neutrophils (Figure 3d; Supplementary Table S4D). Consistent with pathway analysis, targets of cell cycle related E2f7 and Mybl1[39, 56] were more highly expressed in male neutrophils (Figure 3d). Female neutrophils showed higher expression of Foxo4 targets (Figure 3d). Interestingly, the Insulin/Igf1 signaling pathway, which regulates Foxo TF activity, has been linked to multiple sex-dimorphic phenotypes[57, 58].

We next examined sex-dimorphism based on metabolomics and identified a number of pathways with significant sex-bias (Figures 3e; Extended Data Figure 7c; Supplementary Table S4F). Interestingly, metabolic pathways related to nucleotide metabolism were differentially regulated between sexes (Figures 3e; Extended Data Figure 7c; Supplementary Table S4F). Indeed, a number of sex-dimorphic metabolic peaks were predicted to represent nucleotide species (*e.g.* AMP, ATP, GMP; see Supplementary Table S1D). Sex-differences in nucleotide pools are consistent with transcriptomic observations of sex-dimorphism in (i) pathways directly related to nucleotide metabolism, which could lead to direct changes in nucleotide pools, and (ii) pathways responsive to nucleotide levels, such as signaling by Rho-GTPases, which can regulate neutrophil recruitment[59] (Supplementary Table S4A–C,E). Among nucleotides, the impact of adenine derivatives in neutrophils has been studied most extensively. ATP/ADP levels are regulated in neutrophils as a function of activation and 'cellular age'[60]. Adenine nucleotides from neutrophils exert anti-inflammatory effects[61], increase endothelial barrier function, attenuate neutrophil adhesion to endothelial cells, and modulate transendothelial migration[62]. Functional analysis of metabolomic data also suggested significant sex-differences in amino-acid metabolism, such as tryptophan and arginine/proline metabolism (Figures 3e; Extended Data Figure 7c). Interestingly, arginine and tryptophan metabolism play important immunoregulatory roles[63]. However, the final effect of differential metabolite levels from these pathways between sexes will need further investigation.

We then used the Lipid Ontology [LION] framework to analyze sex-dimorphism in lipidomic profiles (Figures 3f, Extended Data Figure 1d, Supplemental Table S4G). Interestingly, male neutrophils were strongly enriched for triacylglycerols [TAG], stored in lipid droplets, whereas female neutrophils were enriched for diacylglycerols [DAG] (Figures 3f; Supplemental Table S4G; Extended Data Figure 1d). Consistently, genes associated to the GO term "negative regulation of lipid storage" were expressed at significantly higher levels in female neutrophils (FDR = 4.33×10^{-3}; Supplemental Table S4C). Lipid droplets are crucial during neutrophil differentiation and as a source for inflammatory mediators[35, 64]. Adipose triglyceride lipase (Atgl), encoded by *Pnpla2*, regulates neutral lipid storage into lipid droplets in neutrophils[65]. Interestingly, *Pnpla2* is expressed at higher levels in female neutrophils (FDR = 0.01; Extended Data Figure 7d; Supplemental Table S1B). Indeed, Atgl catalyzes the conversion of TAG to DAG, consistent with higher levels of DAG in female neutrophils and of TAG in male neutrophils (Figure 3f, Extended Data Figure 1d and Extended Data Figure 7e). Lower levels of *Pnpla2* (mimicking a "masculinized" state) can lead to abnormal neutral lipid accumulation in neutrophils, increased chemotactic ability, and reduced release of proinflammatory lipids[65]. In addition, *Atg7* is crucial for generation of free fatty acids [FFA] from lipid-droplets in neutrophils, and *Atg7*-deficient neutrophils show increased lipid-droplet storage[35]. Consistently, *Atg7* is expressed at higher levels

in female neutrophils (FDR = 0.03; Extended Data Figure 7d; Supplemental Table S1B). Finally, *Lpin1* is crucial for synthesis of DAG from phosphatidic acid, and plays a role in the regulation of inflammation[66]. Consistent with increased DAG levels, *Lpin1* is also expressed at higher levels in female neutrophils (FDR = 0.03; Extended Data Figure 7d; Supplemental Table S1B). Thus, both lipidomics and transcriptomics data suggest that male *vs.* female neutrophils have increased neutral lipid storage (or decreased usage) (Extended Data Figure 7e). Because of the functional importance of lipid droplets, these observations are likely to have deep functional consequences on neutrophil function.

Finally, we performed an integrated analysis using IMPaLA, combining information from transcriptomics, metabolomics and lipidomics (Supplementary Table S4H). We observed joint enrichment of male-biased molecules in pathways linked to cell cycle, DNA metabolism and chromatin-related pathways (Supplementary Table S4H), further supporting the notion that neutrophil chromatin architecture may be regulated in a sex-dimorphic manner. In contrast, female-biased pathways were enriched for lipid-metabolism (Supplementary Table S4H). These joint observations provide an integrated confirmation of our observations for individual “omic” layers. Together, our analyses suggest that major aspects of neutrophils are regulated in a sex-dimorphic fashion and may ultimately underlie sex-differences in immune responses.

Neutrophil chromatin organization changes with sex and age

Our enrichment analyses revealed that chromatin-related pathways were significantly modulated by sex and organismal age in neutrophils, which is expected to result in profound changes in chromatin architecture. Neutrophils hold their chromatin in a compacted polylobular nuclear architecture, which earned them the name of “polymorphonuclear” cells[28, 29]. More than just a gene expression regulatory layer, neutrophil chromatin directly participates in antimicrobial responses through NETs[30, 31]. Thus, chromatin-metabolism differences could lead to profound changes in neutrophil biology. To directly evaluate neutrophil chromatin, we utilized the Assay for Transposon-Accessible Chromatin followed by sequencing [ATAC-seq][67]. ATAC-seq takes advantage of adapter-loaded Tn5 particles inserting into accessible chromatin, yielding information about local chromatin accessibility[67] and higher-order organization[68].

To evaluate chromatin landscapes, we isolated neutrophils from an independent cohort of young (4–5 months) and old (20–21 months) C57BL/6Nia female and male mice and performed ATAC-seq (Figure 4a; Extended Data Figure 8a–h). In contrast with transcriptomic, metabolomic and lipidomic data, MDS analysis on ATAC-seq showed that aging led to better sample separation than sex when examining local differences in chromatin accessibility (Extended Data Figure 8d). In addition, there were substantially more regions with age-related *vs.* sex-dimorphic differential accessibility (Extended Data Figure 8e–h), consistent with numbers of differentially expressed genes with respect to age and sex (Extended Data Figure 1a). Interestingly, enriched GO terms associated to differentially accessible regions with respect to organismal age (FDR < 5%) were mostly associated to regions with increased accessibility, and encompassed terms related to immune response (Supplementary Table S3F). Significantly enriched GO terms for differential

regions with respect to sex (FDR < 5%) were all female-biased, and featured terms related to MAPK signaling and chromatin (Supplementary Table S4I).

Since enrichment analyses suggested that overall aspects of chromatin are differentially regulated with organismal age and sex, we leveraged NucleoATAC[68] to analyze neutrophil chromatin architecture. Interestingly, nucleosome "v-plots" generated revealed a region at ~145–150bp which captured more reads in male *vs.* female neutrophils, regardless of animal age, suggesting global differences in nucleosome packaging (Extended Data Figure 8a). Next, we leveraged indicators linked to chromatin compaction and organization around nucleosomes: (i) nucleosome occupancy, which indicates how frequently a position is occupied by a nucleosome across cells, where higher occupancy is associated to tighter chromatin structure, (ii) nucleosome fuzziness, which indicates how well-positioned the nucleosome is, where fuzzier nucleosomes correspond to looser chromatin, and (iii) inter-dyad distance, which measure DNA length between neighboring nucleosomes, with increased distance associated to looser chromatin.

Occupancy metaplots around transcriptional start sites [TSS] of expressed genes revealed that, regardless of age, male neutrophils showed higher median nucleosomal occupancy compared to female neutrophils (Figure 4b). Similarly, regardless of sex, aging was associated to increased median nucleosomal occupancy (Figure 4c). More generally, male neutrophils had a slight, but significant, increase in nucleosomal occupancy compared to female neutrophils, and median nucleosomal occupancy also slightly increased with organismal age (Figure 4d, Extended Data Figure 8i). We observed decreased nucleosome fuzziness in male *vs.* female neutrophils, as well as in old *vs.* young neutrophils (Figure 4e). Finally, we observed shorter inter-dyad distance in male *vs.* female, as well as old *vs.* young neutrophils (Figure 4f). Together, small (but consistent) increases in occupancy, decreases in fuzziness and decreases in inter-dyad distance, are indicative of an overall more compacted chromatin architecture in male *vs.* female and old *vs.* young neutrophils. Finally, when analyzing ATAC-seq fragments at accessible regions (including subnucleosomal fragments), we observed lower median fragment length in male and old neutrophils (Extended Data Figure 8j). While this observation may seem contradictory, overall shorter ATAC-seq fragments in the libraries may result from relatively "more accessible" nucleosome-free regions in the context of overall tighter chromatin.

To independently evaluate chromatin compaction, we leveraged our RNA-seq to examine transcription of repeats (Extended Data Figure 8k–l; Supplementary Table S1G,H). Eukaryotic genomes contain large proportions of repeats, including transposons, whose transcription is usually tightly repressed through compaction[69]. Consistent with a more compact chromatin architecture, male neutrophils showed lower transcription of repeats *vs.* females (350 female-biased elements *vs.* 12 male-biased; Extended Data Figure 8l; Supplementary Table S1H). Similarly, old neutrophils also showed lower transcription of repeats *vs.* young neutrophils (115 elements downregulated *vs.* 27 upregulated with age; Extended Data Figure 8k; Supplementary Table S1G). Interestingly, chromatin decompaction is a limiting step of NETosis[70], suggesting that baseline differences in chromatin compaction in neutrophils of different ages and sex may impact the dynamics

and timeline of NETosis. However, chromatin profiling alone cannot predict the direction in which NETosis could be affected.

Based on transcriptome and ATAC-seq results, we predicted that NETosis inducibility should be regulated as a function of sex and organismal age. We evaluated NETosis inducibility in neutrophils isolated from young *vs.* old, female *vs.* male mice (Figure 4g–i). We used flow cytometry to quantify cells with extracellularized DNA (*i.e.* NETosed or NETosing cells), after a 2h incubation in the presence of Phorbol 12-myristate 13-acetate [PMA], a known activator of NETosis, compared to vehicle (Figure 4g). We first evaluated NETosis induction on unstimulated neutrophils (Figure 4h). NETosis inducibility was significantly increased with organismal age in female cells ($p = 4.5\times10^{-5}$), while higher animal-to-animal variability and no significant change were observed in male cells (Figure 4h). Young male neutrophils showed higher NETosis capacity than young female neutrophils ($p = 0.057$), a trend reversed with organismal aging, with old female neutrophils showing highest NETosis inducibility ($p = 0.029$; Figure 4h).

Increased NETosis in neutrophils from older female mice may seem contradictory with previous reports of decreased NETosis with organismal aging[13, 14]. To note, previous studies evaluated NETosis after *in vitro* TNFα priming[13] or in conditions known to mimic TNFα priming[14, 71], and did not evaluate sex as a biological variable. TNFα is a pro-inflammatory cytokine and a potent inducer of NETosis[13]. To evaluate how TNFα-priming may impact NETosis across groups, we also performed NETosis experiments on cells pre-treated with 10ng/mL TNFα (Figure 4i). Although TNFα-priming yielded noisier data, NETosis inducibility was blunted with organismal age in female cells stimulated with TNFα (Figure 4i). In contrast, TNFα-primed male neutrophils trended towards decreased inducibility of NETosis with organismal age ($p = 0.092$; Figure 4i). In TNFα-primed conditions, young male *vs.* female neutrophils no longer showed differences in NETosis inducibility, but old female neutrophils still showed the highest overall NETosis inducibility (Figure 4i). Together, we find that NETosis is differentially modulated as a function of organismal age and sex, consistent with observed differences in chromatin architecture.

Machine-learning predicts features of neutrophils regulation

To understand whether age-related and sex-dimorphic gene expression can be predicted from genomic sequence, chromatin and/or regulation by TFs, we took advantage of machine-learning (Figure 5a–c, Figure 6a–c, Extended Data Figure 9a–f). Machine-learning can help (i) to determine whether features contain information predictive of a state of interest (*e.g.* sex-dimorphic or age-regulated expression), and (ii) to identify predictive features of such states. We used seven algorithms to learn models discriminating between (i) up- and down-regulated expression with age, and (ii) male- or female-biased gene expression (*i.e.* conditional inference Trees [cTree], Linear Discriminant Analysis [LDA], neural networks [NNET], Logistic Regression [LogReg], random forests [RF], support vector machines [SVM], and gradient boosting [GBM]). The models were trained with features related to (i) genomic sequence (*e.g.* GC-richness), (ii) chromatin accessibility (*e.g.* changes in ATAC-seq promoter accessibility), and (iii) TF target genes (*i.e.* same as used with GSEA).

We first evaluated our ability to discriminate between genes upregulated *vs.* downregulated during aging in neutrophils (Figure 5a). Our models assigned genes to the correct transcriptional change with age >64% of the time on testing data (Figure 5b; Supplementary Table S5A), significantly above random (50%). High accuracy suggests that clear biological features differentiate between genes that tend to be up- *vs.* downregulated with aging.
To assess which features were most predictive of age-related changes, we examined predictor contribution from RF and GBM models, which provide native evaluation of feature importance (Figure 5c; Supplementary Table S5B). Consistent with the tight link between chromatin and gene expression[72], the average promoter ATAC-seq signal (*i.e.* describing how "open" the promoter is), as well as the fold difference in ATAC-seq signal between young and old neutrophils (*i.e.* age-related changes in openness) were among the top predictors for age-related changes (Figure 5c; Supplementary Table S5B). Key predictors also included CG/CpG content in the promoter and gene sequences (Figure 5c), which is consistent with our previous work identifying promoter CpG content as a top predictor of age-related gene expression in mouse tissues[18]. Cytosines in CpG configuration are the primary targets of DNA methylation[73]. CpG DNA methylation [DNAme], catalyzed by DNA-methyltransferases (*i.e.* writers), can be removed by TET family proteins (*i.e.* erasers) and is interpreted through recognition by methyl-CpG binding proteins (*i.e.* readers)[73]. Consistent with the notion that the predictive power of CpG content is related to changes in CpG methylation regulation, RNA-seq revealed significant downregulation with organismal aging of DNA-methyltransferase encoding *Dnmt1*, demethylation-catalyzing TET encoding *Tet1* and *Tet2*, as well as methyl-CpG binding domain proteins encoding *Mbd4* and *Mbd5* (FDR < 5%; Supplementary Table S1A). The presence of putative age-related changes in DNAme is consistent with the notion that DNAme patterns can serve as "aging clocks"[74].

Key predictors of age-related expression changes also included whether a gene was a target of specific TFs: Stat5a, Mtf2, Sirt6, Foxo1, *etc.* (Figure 5c; Supplementary Table S5B). Although causality cannot be inferred from machine-learning, predictors provide a list of candidate drivers/mediators of programs related to organismal aging. Only a subset of top TF predictors were themselves differentially regulated with aging (*e.g. Stat5a, Mtf2, Nod2*; Extended Data Figure 9g; Supplementary Table S1A). Thus, it is possible that the activity of TF predictors without RNA-level regulation may occur through post-translational regulation. Interestingly, Stat5a mediates the effects of GM-CSF on granulocyte differentiation[75], and is crucial for mature neutrophils survival[76]. Although the role of Mtf2 in neutrophils has not been studied, Mtf2 interacts with Jarid2 (another top predictor) to promote repressive H3K27 methylation[77], which mediates recruitment to unmethylated CpGs[78]. Nod2 is a pattern recognition receptor that recognizes muramyl dipeptide, the minimal common motif of bacterial peptidoglycans[79]. Although Nod2 is not a TF, it has profound transcriptional effects on gene expression, with target genes including cytokines and chemokines[80, 81]. Indeed, Nod2 is an important contributor of neutrophil-mediated innate immunity[81].
Sirt6 is a histone deacetylase tightly linked to the regulation of mammalian aging and longevity[82, 83]. Sirt6 can limit inflammation by deacetylating the promoters of NF-kB targets[84] and reducing cytokine production[85]. Consistently, *Sirt6* knockout mice show liver inflammation with neutrophil infiltration[86]. Thus, changes in activity for top predictive TFs may drive aspects of age-related transcriptional remodeling.

We next asked whether sex-dimorphic gene expression could be predicted from genomic information, local chromatin states and/or TF regulation (Figure 6a). Importantly, as an additional feature, we also included the chromosomal location of a gene (*i.e.* sex-chromosomes *vs.* autosomes). Our models assigned genes to the correct sex-based expression bias >70% of the time on held-out testing data (Figure 6b; Supplementary Table S5C), consistent with the notion that sex-biased genes share a common regulatory signature. To understand which features were most predictive of male- or female-biased expression, we again examined predictor contribution from RF and GBM models (Figure 6c; Supplementary Table S5D). Importantly, being located on a sex chromosome (X or Y) was a poor predictor of sex-dimorphic gene expression (166th combined importance rank; Supplementary Table S5D), consistent with the fact that genetic context was not a crucial driver (Extended Data Figure 1a). Similar to our age-related models, the average promoter ATAC-seq signal and the fold change between females *vs.* males in ATAC-seq signal were also top predictors for sex-biased gene expression (Figure 6c; Supplementary Table S5D). The GC/CpG content of promoter and genes sequences also showed strong predictive power, consistent with the sex-dimorphic expression of DNAme regulators (*i.e.* male-biased expression for *Dnmt1* and *Tet3*; Supplementary Table S1B).

Finally, we asked which TFs were most predictive of sex-dimorphic gene expression in neutrophils (Figure 6c; Supplementary Table S5D). Being a known target of Foxm1, Sirt6, Mtf2 or Mybl2 was highly predictive of male *vs.* female neutrophil-biased gene expression, suggesting that these may drive aspects of the sex-dimorphic neutrophil biology. Similar to above, only a small subset of top predictors from our models were themselves significantly regulated at the transcriptional level (e.g. *Foxm1*, *Irf8*; Extended Data Figure 9h; Supplementary Table S1B). Although its role hasn't been explored in neutrophils, Foxm1 regulates the expression of cell cycle-related genes[87] and is highly expressed in late committed neutrophil precursors[40]. The transcription factor Mybl2 also regulates cell cycle-related genes[88], and can modulate differentiation and cell fate decision of myeloid progenitors[89]. Thus, top predictors of sex-dimorphic neutrophil gene expression Foxm1 and Mybl2 might be linked to observed sex-dimorphic expression of cell cycle and chromatin-related genes (Figure 3, Extended Data Figure 7). Being a target of Sirt6 was also predictive of sex-dimorphic gene expression, in line with sex-dimorphic phenotypes of Sirt6 knock-out and overexpression mice[82, 83]. In addition, consistent with sex-dimorphism in lipid storage (Figure 3f), Sirt6 is tightly linked to lipid metabolism[90], and can limit lipid droplet accumulation in foam cells[91]. In addition, Sirt6 activity can be directly regulated by FFAs (*e.g.* myristic, oleic and linoleic acid)[92]. Consistently, female neutrophils have higher levels of FFAs, including FFA(14:0) and FFA(18:2) (*i.e.* myristic and linoleic acid), and may thus have higher basal Sirt6 activity levels (Supplementary Table S1E,F). Thus, our machine-learning analysis reveals candidate regulators that may drive neutrophil sex-dimorphism and will deserve further investigation.

Primary granule differences in female *vs.* male neutrophils

Intriguingly, when analyzing the top genes with the largest fold-difference between male *vs.* female neutrophils, we noticed that genes encoding primary neutrophil granule components showed top male-biased expression (*e.g. Elane*, *Mpo*, *Prtn3* and *Ctsg*; Supplementary

Table S1B), suggesting potential sex differences in granule loading. Thus, we investigated potential differences in granule biogenesis (Figure 7a–b, Extended Data Figure 10a–d). Neutrophils store a number of proteases and antimicrobial proteins in (i) primary/azurophilic granules, (ii) secondary/specific granules, and (iii) tertiary/gelatinase granules. To unbiasedly assess whether neutrophil granule biology is sex-dimorphic, we compiled a list of granule components from the literature (Supplementary Table S6). Consistent with our first observation, GSEA revealed a robust trend for increased RNA expression of primary granule-related genes in male *vs.* female neutrophils, regardless of age (Figure 7a–b). In contrast, no significant enrichments were observed for genes encoding components of secondary or tertiary granules (FDR > 5%; Extended Data Figure 10a–d). Importantly, we confirmed that protein levels of neutrophil elastase Elane were higher in young males *vs.* young females by Western blot ($p = 3.9\times10^{-3}$ in two-sided Wilcoxon's test between young females and male samples), although this sex-difference disappeared in older animals (Extended Data Figure 5d,e).

Neutrophil degranulation is a key aspect of the response of neutrophils to pathogens[93], and mice without a functional copy of *Elane* have increased mortality upon sepsis[94]. However, excessive levels of circulating neutrophil elastase can be deleterious, amplifying septic shock[95]. Based on RNA-seq, we hypothesized that higher *Elane* expression in neutrophils could lead to increased Elane circulating levels, both in basal conditions and upon an immune challenge. To test this hypothesis, we obtained female and male young adult C57BL/6J mice, and injected them with sterile PBS or LPS (a major component of gram-negative bacteria cell wall), for 1–6 hours, to mimic a septic state[96] (Figure 7c). Interestingly, males showed significantly higher levels of serum neutrophil elastase at 3 and 6 hours post LPS exposure (Figure 7d), and in the PBS-injected controls (Figure 7d,e). Thus, young males had overall higher serum protein levels of Elane.

Finally, we then took advantage of a published proteomics dataset of human blood neutrophils from 68 healthy donors[97]. Since the biological sex of human donors was not specified, we used the reported protein levels of DDX3Y, a protein encoded on the Y chromosome, as a proxy for the likelihood that the sample was derived from a male donor (*i.e.* higher levels of DDX3Y associated with males). Consistent with our mouse RNA-seq and serum ELISA, we found significant correlation between DDX3Y levels (*i.e.* likelihood of the sample coming from a male donor) and expression of primary granule proteins ELANE, MPO and CTSG, although not of PRTN3 (Figure Extended Data Figure 10e–g). Thus, our results suggest that neutrophils derived from human males have higher protein expression of key primary granule components. These observations suggest that, at least for these components, transcriptomic trends are predictive of protein-level trends, and that the male-bias in primary granule components observed in our mouse data may be conserved in humans.

Discussion

A resource for the study of neutrophils across sex and aging

We have generated transcriptomic, metabolomic, lipidomic and epigenomic datasets using bone marrow neutrophils from young and old, female and male animals. To our knowledge,

this dataset is the largest multi-omic dataset for the study of neutrophils and is one of the rare cases to include both sexes and organismal aging, rather than focusing only on one sex or age group. Using this resource, we observed that (i) neutrophils are extremely sex-dimorphic, and that (ii) organismal age leads to large scale transcriptomic and epigenomic remodeling of neutrophils. Interestingly, when analyzed separately, males had > 10-fold more significantly regulated genes with age than females, suggesting that the molecular rate of neutrophil aging differs between sexes. Observed changes may likely be downstream of signals that drive aging itself, but these changes will impact immune responses in aged animals, participating in immune dysfunction.

We then predicted increased release of neutrophil elastase in males in control and sepsis-like conditions. Excess release of neutrophil elastase is known to exacerbate inflammation and cause tissue damage[98]. Thus, this resource should help open new avenues of research and identify candidate mediators that underlie sex-differences in lifelong immunity. Future studies should investigate how the differences in bone marrow neutrophils are maintained, erased or amplified in circulating blood neutrophils.

Sex and aging influence neutrophil chromatin metabolism

We observed that regulation of chromatin metabolism is a hallmark of neutrophil aging, and a key aspect with sex-dimorphic regulation. Far from being a mere regulatory layer for gene expression, chromatin organization has profound implications on NETosis[8]. Our analyses suggest that female neutrophils have an overall “looser” chromatin, associated to the transcriptional upregulation of a number of transposable elements [TEs]. Conversely (and regardless of sex), neutrophils from old individuals show increased chromatin condensation accompanied by reduced TE transcription. This contrasts with observation of age-related TE derepression in other contexts[19], and may reflect the unique neutrophil biology. Thus, it will be important to elucidate the mechanism driving differences in NETosis between sexes and throughout lifespan, with implications in aberrant chronic age-related inflammation[10].

Machine-learning as a powerful candidate-identification tool

By using machine-learning, we showed that both age-regulation and sex-dimorphism in gene expression can be predicted accurately. The high accuracy of our models supports the notion of coordinated differences between (i) genes induced *vs.* repressed during aging, and (ii) genes expressed in a sex-dimorphic manner. Among important predictors of transcriptional states, we identified regulators whose activity change during organismal aging may underlie “omic” profile remodeling throughout life *(e.g.* Foxo1, Sirt6). We also identified putative mediators of sex-biased gene expression of neutrophils (*e.g.* Foxm1, Mybl2). Although machine-learning does not provide information about causality, predictors represent candidate mediators that could help shape neutrophil landscapes with aging or as a function of sex. Thus, it will be important to elucidate the potential role of these predictors to understand the emergence of age-related and sex-dimorphic phenotypes.

Neutrophils as mediators for sex-differences in immune aging

Accumulating evidence has shown that, even outside of reproduction, mammalian biology is extremely sex-dimorphic[99]. This is especially relevant to aging, with large sex-differences

in baseline lifespan and in response to pro-longevity interventions[58]. Although this has not been broadly investigated with aging, pioneering studies have started to compare male and female cells, revealing profound sex-dimorphism in gene regulation[21, 22]. Consistently, accumulating evidence has shown that immune responses differ between sexes[100, 101].

Sex-dimorphism in immunity is exemplified in the current health crisis, with men representing the majority of severe cases and deaths from COVID-19[102]. Interestingly, NETs may drive aspects of inflammatory disease, lead to tissue damage[8, 30], and contribute to severe COVID-19[103]. In addition, neutrophil dysfunction has been linked to the pathogenesis of a number of chronic diseases (*e.g.* macular degeneration[104], stroke[105], obstructive pulmonary disease[106], atherosclerosis[107], cancer[108], *etc.*). Thus, sex differences in neutrophils could constitute targets to optimize immune responses throughout life and help tailor therapeutics to men and women.

Methods

Mouse husbandry

All animals were treated and housed in accordance with the Guide for Care and Use of Laboratory Animals. All experimental procedures were approved by the University of Southern California's Institutional Animal Care and Use Committee (IACUC) and are in accordance with institutional and national guidelines. Samples were derived from animals on approved IACUC protocols #20770, #20804 and #21004.

For 'omics' analyses, male and female C57BL/6Nia mice (4–5 and 20–24 months old animals) were obtained from the National Institute on Aging (NIA) colony at Charles Rivers. For the sepsis assays in young animals, male and female C57BL/6J mice (3–4 months old animals) were obtained from Jackson Laboratories. Both Charles Rivers and Jackson Laboratories have specific-pathogen-free (SPF) facilities. Animals were acclimated at the SPF animal facility at USC for 2–4 weeks before any processing. The facility is on a 12-hour light/dark cycle, and animal housing rooms are maintained at 72°F and 30% humidity. All animals were euthanized between 8–11am for 'omics' experiments, flow cytometry and NETosis assays. For the sepsis model experiments, animals were injected in the morning, and euthanized between 4–6pm. In all cases, animals were euthanized using a "snaking order" across all groups to minimize batch-processing confounds due to circadian processes (including potential confounds due to neutrophil cellular "age"). All animals were euthanized by CO_2 asphyxiation followed by cervical dislocation.

Isolation of primary neutrophils from mouse bone marrow

The long bones of each mouse were harvested and kept on ice in D-PBS (Corning) supplemented with 1% Penicillin/Streptomycin (Corning) until further processing. Muscle tissue was removed from the bones, and the bone marrow from cleaned bones was collected into clean tubes[110]. Red blood cells from the marrow were removed using Red Blood Cell Lysis buffer (Miltenyi Biotec #130–094-183), according to the manufacturer's instructions, albeit with no vortexing step to avoid unscheduled neutrophil activation. The suspension was filtered on 70μm mesh filters (Miltenyi Biotec #130–110-916) to retain only single

cells for downstream processing. Neutrophils were isolated from other bone marrow cells using magnetic-assisted cell sorting (Miltenyi Biotec kit #130–097-658). Viability and yield were assessed using trypan blue exclusion and an automated COUNTESS cell counter (Thermo-Fisher Scientific). Purified cells were pelleted at 300g and snap-frozen in liquid nitrogen until processing for RNA, lipid or metabolite isolation.

Neutrophil purity estimates by flow cytometry

We used aging C57BL/6Nia mice from two independent cohorts to estimate potential differences in neutrophil purity with respect to sex and age. After an Fc-blocking step (Miltenyi Biotec #130–092-575), MACS-purified neutrophils were then stained using APC-Ly6G (Invitrogen #17–9668-80) and Vioblue-Cd11b (Miltenyi Biotec #130–113-238) at a 1:50 dilution according to the manufacturer's instructions. Stained cells were then analyzed by flow cytometry on a MACS Quant Analyzer 10 (Miltenyi Biotec). Flow cytometry results were processed using the FlowLogic V7 software. Purity of MACS-isolated bone marrow neutrophils in young and aged male and female animals are reported in Extended Data Figure 3. Raw cytometry data was deposited on Figshare (doi.org/10.6084/m9.figshare.14043932.v1).

Purified neutrophil heterogeneity estimate by flow cytometry

We used flow cytometry analysis to evaluate the heterogeneity/maturity of our isolated neutrophils from two independent cohorts of aging C57BL/6Nia mice. We used a panel of antibodies designed to evaluate population heterogeneity of cells purified by MACS based on defined subpopulations of neutrophils in the literature[111, 112, 113] (see below). Specifically, among live cell singlets, pro-neutrophils were defined as c-Kit$^+$Ly6g$^-$Cd81$^+$, with subpopulations of pro-neutrophil 1 defined as c-Kit$^+$Ly6G$^-$Cd81$^+$CD11b$^-$CD106$^-$ and pro-neutrophil 2 as c-Kit$^+$Ly6G$^-$Cd81$^+$CD11b$^+$CD106$^+$. Pre-neutrophils were defined as Cd11b$^+$Ly6G$^+$c-Kit$^+$Cxcr4$^+$ cells. Immature neutrophils were defined as CD11b$^+$Ly6G$^+$c-Kit$^-$Cxcr4$^-$Cxcr2$^-$ cells, and mature neutrophils as CD11b$^+$Ly6G$^+$c-Kit$^-$Cxcr4$^-$Cxcr2$^+$. Fresh *vs.* "aged" subsets of mature neutrophils were defined respectively as CD11b$^+$Ly6G$^+$c-Kit$^-$Cxcr4$^-$Cxcr2$^+$CD62L$^+$ *vs.* CD11b$^+$Ly6G$^+$c-Kit$^-$Cxcr4$^-$Cxcr2$^+$CD62L$^-$ cells.

Prior to analyzing compositional heterogeneity on MACS-purified neutrophils, to account for spill over from different lasers, compensation was performed using appropriate compensation beads (Miltenyi Biotec #130–104-693 for Miltenyi antibodies; ThermoFisher # 01–3333-42 for others). The compensation file was saved and loaded prior to analyzing neutrophils. Compensation was rerun anytime at least one fresh vial of antibody had to be used for the staining experiment.

Antibodies used for this heterogeneity panel were:

- CD184 (CXCR4) - PE-Vio770 (clone REA107; Miltenyi Biotec 130–102-914) at 1:10 dilution
- CD81 - PE (clone EAT2; Miltenyi Biotec 130–102-632) at 1:10 dilution

- CD11b – Vioblue (clone REA592; Miltenyi Biotec 130–113-810) at 1:50 dilution
- Ly6G - PerCP-Vio700 (clone REA526; Miltenyi Biotec 130–117-500) at 1:50 dilution
- CD182 (CXCR2) - APC-Vio770 (clone REA942; Miltenyi Biotec 130–115-637) at 1:50 dilution
- CD62L – FITC (clone REA828; Miltenyi Biotec 130–112-835) at 1:50 dilution
- CD106 (VCAM-1) – APC (clone REA971; Miltenyi Biotec 130–116-324) at 1:50 dilution
- CD117 (c-kit) – Brilliant Violet 510 (clone ACK2; Biolegend 135119) at 1:20 dilution

After isolation by MACS, 2.5×10^5 cells were washed once by adding 1mL of PBS/EDTA 0.1% BSA (*i.e.* MACS resuspension buffer) in a 5mL polystyrene round bottom tube (Falcon #352054), then centrifuged 300g for 10 minutes at 4°C. After an Fc-blocking step (Miltenyi Biotec #130–092-575), MACS-purified neutrophils were then stained with antibodies for 20 minutes at 4°C, and excess antibody was washed away using resuspension buffer. Stained cells were then analyzed by flow cytometry on a MACS Quant Analyzer 10 (Miltenyi Biotec), and flow cytometry data was analyzed using FlowLogic V7. Gating was determined using fluorescence-minus-one [FMO] controls for each color used in the experiment to ensure that positive populations were solely associated with the antibody for that specific marker (Extended Data Figure 4a). Due to the low amount of c-kit$^+$ events in MACS-purified neutrophils, we also ran whole bone marrow (pooled by group in one cohort) with the same scheme to confirm that positive labelling by this antibody occurs normally on bone marrow cells prior to purification (Extended Data Figure 4b). Both sets of raw cytometry data, including FMO controls and compensation files, were deposited to Figshare (doi.org/10.6084/m9.figshare.14043929.v1, doi.org/10.6084/m9.figshare.14043938.v1).

Estimate of neutrophil proportion in bone marrow in young female and male mice

We used aging C57BL/6Nia mice from two independent cohorts to estimate potential differences in neutrophil proportions within nucleated bone marrow cells with respect to sex and age. An aliquot of bone marrow cell suspension was obtained after bone marrow extraction, red blood cell lysis and filtration on 70μm mesh filters (see above). Cell composition analysis was obtained using the Hemavet 950FS at the USC Leonard Davis School of Gerontology mouse phenotyping core. Percentage of cells was used instead of absolute cell numbers to avoid confounding results due to animal size.

Evaluation of cell-cycle patterns of MACS-purified neutrophils by flow cytometry

We used aging C57BL/6Nia mice from two independent cohorts to estimate cell cycle proportions of MACS-purified neutrophils with respect to sex and age. We utilized a standard method using DNA content, as measured by propidium iodide staining of fixed cells, to estimate the phases of the cell cycle (*i.e.* G0/G1, S and G2/M). For each biological

sample, 5×10^5 cells were aliquoted and fixed with 70% Ethanol at −20°C overnight. The next day, cells were washed with DPBS [Corning], and nuclear DNA was stained for 30 minutes at room temperature in labelling buffer (50μg/mL propidium iodide [Alfa Aesar], 100μg/mL RnaseA [Invitrogen], 0.05% Triton X-100 [Sigma] in DPBS [Corning]). Stained cells were then analyzed by flow cytometry on a MACS Quant Analyzer 10 (Miltenyi Biotec), and flow cytometry data was analyzed using FlowLogic V7. Raw cytometry data was deposited to Figshare (doi.org/10.6084/m9.figshare.14043926.v1).

RNA purification and RNA-seq library preparation

For RNA isolation, frozen cell pellets were resuspended in 1mL of Trizol reagent (Thermo-Fisher), and total RNA was purified following the manufacturer's instructions. RNA quality was assessed using the Agilent Bioanalyzer platform at the USC Genome Core using the RNA Integrity Number (RIN). 500ng of total RNA was subjected to ribosomal-RNA depletion using the NEBNext rRNA Depletion Kit (New England Biolabs), according to the manufacturer's protocol. Strand specific RNA-seq libraries were then constructed using the SMARTer Stranded RNA-seq Kit (Clontech), according to the manufacturer's protocol. Libraries were quality controlled on the Agilent Bioanalyzer 2100 platform at the USC Genome Core before multiplexing the libraries for sequencing. Paired-end 75bp reads were generated on the Illumina NextSeq500 platform at the SC^2 Core at CHLA (original cohort) or paired-end 150bp reads were generated on the Illumina HiSeq-Xten platform at the Novogene Corporation (USA) (replicate cohort).

RNA-seq analysis pipeline

To best mimic the first RNA-seq cohort, paired end 150bp reads from the replicate cohort of neutrophil RNA-seq were hard-trimmed to 75bp using Fastx Trimmer. Both sets of paired-end reads were processed using Trimgalore 0.4.4 (github.com/FelixKrueger/TrimGalore) (i) to retain only high-quality bases with phred score > 15, and (ii) to eliminate biases due to priming by hard clipping the first 6 bases of each read. Only pairs with both reads retaining a length of > 45bp after trimming were retained for further processing. Trimmed reads were mapped to the mm10 genome reference using STAR 2.5.0a[114]. Read counts were assigned to genes from the UCSC mm10 reference using subread1.5.3[115] and were imported into R to perform differential gene expression analysis. Based on general RNA-seq processing guidelines, only genes with mapped reads in at least 6/16 RNA-seq libraries were considered to be expressed and retained for downstream analysis. Due to high sample-to-sample variability, we used surrogate variable analysis to estimate and correct for unwanted experimental noise[116]. R package 'sva' v3.34 was used to estimate surrogate variables, and the removeBatchEffect function from 'limma' v3.42.2 was used to regress out the effects of surrogate variables and RNA-integrity differences (RIN scores) from raw read counts. The 'DESeq2' R package (DESeq2 1.26.0) was used for further processing of the RNA-seq data in R[117]. Importantly, sex was encoded as a categorical variable (female *vs.* male), and age was encoded as a continuous numerical variable. Genes with a false discovery rate < 5% were considered statistically significant and are reported in Supplementary Table S1A–B.

Dimensionality reduction for exploratory data analysis

To perform Multidimensional Scaling (MDS) analysis[118], we used a distance metric between samples based on the Spearman's rank correlation value (1-Rho), which was then provided to the core R command 'cmdscale'. Dimensionality reduction was applied to pre-normalized data, as described in relevant sections.

Replicate and public neutrophil RNA-seq comparison

To assess the robustness of transcriptional changes linked to biological sex and/or organismal age, we used (i) a small replicate RNA-seq cohort of primary bone marrow neutrophils with all four conditions, (ii) a dataset from mouse spleen neutrophils from young adult female *vs.* males from the ImmGen consortium (6 weeks-old animals; GEO Datasets GSE124829)[22] and (iii) a dataset from human blood neutrophils (ages unknown; GEO Datasets GSE145231)[24] (Extended Data Figure 2a,b). Reads were mapped to mm10 and hg38 respectively using STAR, and reads were summarized to genes using subread as before. DESeq2 normalized fold-changes were then used to estimate differential gene expression as a function of age and of sex. For mouse datasets, the comparison directly assessed the DESeq2 normalized fold-changes for genes with FDR <5% in the original cohort RNA-seq. For the human dataset, orthologs of significant mouse genes in humans were identified using the R 'biomaRt' 2.42.1 package (accessed 2020–12-18), and DESeq2 normalized fold-changes were then compared.

Putative Protein-Protein Interaction [PPI] network analysis

Genes with significant regulation according to our DEseq2 analysis (FDR < 5%) were used as input for network analysis with NetworkAnalyst 3.0[119]. For age-related gene regulation, significant genes and DEseq2 calculated $\log_2$(fold-change) were used as input for a single network analysis. For sex-dimorphic gene regulation, the female- and male-biased gene lists were used as separate inputs for the analysis. To avoid network clusters due to sex-chromosome encoded genes, only significant autosomal genes were included in the sex-dimorphism gene expression networks. In both cases, NetworkAnalyst was set up to use PPI information derived from IMEx/InnateDB data, a knowledgebase specifically geared for analyses of innate immune networks[109], to construct putative PPI networks. In each case, the largest subnetwork determined by NetworkAnalyst was used in figures and analyses.

Functional enrichment analysis (transcriptomics)

We used the Gene Set Enrichment Analysis (GSEA) paradigm[120] through the 'phenotest' 1.34.0 R package. Gene Ontology term annotation were obtained from ENSEMBL through Biomart (Ensembl 99; downloaded on 2020–04-10), and gene-term association with only author statement support (GO evidence codes 'TAS' and 'NAS') or unclear evidence (GO evidence code 'ND') were filtered out. Other annotations were obtained from the Molecular Signature Database v7.0 (*e.g.* Reactome, KEGG)[120, 121] and the Harmonizome Database (*e.g.* ChEA, JASPAR, ENCODE, GEO TF targets; accessed 2020–03-25)[122]. To improve target coverage, we summarized putative transcription factor [TF] targets, including FOXO TF targets compiled in our previous study[18], so as to have a reduced, unique, and non-redundant list of TF targets summarized from all these sources. The DEseq2 t-statistic was

used to generate the ranked list of genes for functional enrichment analysis, both for the sex and aging effects. For ease of reading, only the top 10 most significant pathways with negative NES and top 10 most significant pathways with positive NES are shown in figures if more than that pass the FDR < 5% significance threshold. All significant gene sets are reported in Supplementary Tables S3 (aging) and S4 (sex). In parallel, functional enrichment was also independently assessed using the Ingenuity Pathway Analysis portal, using genes with a significant male or female bias (FDR < 5%).

Western blot analysis of Padi4 and Elane protein levels

To prepare neutrophil lysates, ~5 million cells were collected from aging C57BL/6Nia mice from two independent cohorts (n = 9 animals per group). Flash frozen cell pellets were resuspended in 200 μL ice-cold lysis buffer (10 mM Tris-HCl pH 8.0, 1% SDS, 1x Halt Protease and Phosphatase Inhibitor Cocktail [Life Technologies # 78442]) and incubated on ice for 30 minutes. Samples were sonicated (Fisher Scientific # FB120; 60% power, 30 sec ON/ 120 sec OFF, 4 cycles) and centrifuged at 16,000g for 20 minutes at 4°C. Supernatant was collected and boiled in 4x Laemmli Sample Buffer (Biorad # 1610747). Proteins were separated on 10% SDS-PAGE gels and wet-transferred onto PVDF membranes (GE Healthcare # 10600021). To assess loading and transfer efficiency, membranes were stained using the Ponceau S solution (Sigma P7170) for 2 minutes at room temperature. Membranes were blocked using 5% milk (Carnation) in 1xTBST buffer (TBS [Alfa Aesar J62938], supplemented with 0.05% Tween-20 [Bio-rad #161–0781]) for 1 hour at room temperature. Membranes were incubated with primary antibodies diluted in 5% milk in TBST (anti-β-Actin: Cell Signaling D6A8 at 1:5,000 dilution; anti-ELANE: Abcam ab68672 at 1:1,000 dilution; and anti-PADI4: Abcam ab96758 at 1:3,000 dilution) for 16 hours at 4°C. After three-5 minute washes using 1xTBST buffer, membranes were incubated with an HRP-conjugated secondary antibody (Goat Anti-Rabbit IgG H&L, Abcam ab205718 at 1:10,000 dilution) for 1 hour at room temperature. For visualization, membranes were treated with chemiluminescence solution according to manufacturer's manual (Biorad # 1705062 and Thermo Scientific # 34580) and images were taken using Azure Biosystems c280.

For band intensity quantification, ImageJ (version 1.53) was used. Grayscale converted images were imported to ImageJ and intensity was measured from all bands. Background intensity was subtracted from each measurement. Anti-β-Actin-relative values from each membrane were normalized by the median value of the specific membrane to mitigate membrane-specific variations.

All raw original images and cropped equivalents, as well as ImageJ quantification, have been made available on Figshare (https://doi.org/10.6084/m9.figshare.14154665.v1) and as a source data file for Extended Data Figure 5.

Chemicals for LC-MS

LC-MS-grade solvents and mobile phase modifiers were obtained from Fisher Scientific (water, acetonitrile, methanol, methyl tert-butyl ether) and Sigma−Aldrich (ammonium acetate).

Metabolite and lipid extraction from neutrophils.

Metabolites and lipids were extracted from neutrophil cell pellets and analyzed in a randomized order. Extraction was performed using a biphasic separation protocol with ice-cold methanol, methyl tert-butyl ether (MTBE) and water[123]. Briefly, 300μL of methanol spiked-in with 54 deuterated internal standards provided with the Lipidyzer platform (SCIEX, cat #5040156, LPISTDKIT-101) was added to the cell pellet, samples were vigorously vortexed for 20 seconds and sonicated in a water bath 3 times for 30 seconds on ice. Lipids were solubilized by adding 1000μL of MTBE and incubated under agitation for 1h at 4°C. After addition of 250μL of ice-cold water, the samples were vortexed for 1 min and centrifuged at 14,000g for 5 min at 20°C. The upper phase containing the lipids was then collected and dried down under nitrogen. The dry lipid extracts were reconstituted with 300μL of 10 mM ammonium acetate in 9:1 methanol:toluene for analysis. The lower phase containing metabolites was subjected to further protein precipitation by adding 4 times of ice-cold 1:1:1 isopropanol:acetonitrile:water spiked in with 17 labeled internal standards and incubating for 2 hours at −20°C. The supernatant was dried down to completion under nitrogen and re-suspended in 100μL of 1:1 MeOH:Water for analysis.

Untargeted LC-MS metabolomics.

Data acquisition.—Metabolic extracts were analyzed four times using hydrophilic liquid chromatography (HILIC) and reverse phase liquid chromatography (RPLC) separation in both positive and negative ionization modes as previously described[124]. Data were acquired on a Thermo Q Exactive plus mass spectrometer equipped with a HESI-II probe and operated in full MS scan mode. MS/MS data were acquired on pool samples consisting of an equimolar mixture of all the samples in the study. HILIC experiments were performed using a ZIC-HILIC column 2.1×100 mm, 3.5μm, 200Å (Merck Millipore) and mobile phase solvents consisting of 10mM ammonium acetate in 50/50 acetonitrile/water (A) and 10 mM ammonium acetate in 95/5 acetonitrile/water (B). RPLC experiments were performed using a Zorbax SBaq column 2.1 × 50 mm, 1.7 μm, 100Å (Agilent Technologies) and mobile phase solvents consisting of 0.06% acetic acid in water (A) and 0.06% acetic acid in methanol (B). Data quality was ensured by (i) injecting 6 and 12-pool samples to equilibrate the LC-MS system prior to run the sequence for RPLC and HILIC, respectively, (ii) sample randomization for metabolite extraction and data acquisition, and (iii) checking mass accuracy, retention time and peak shape of internal standards in every samples.

Data processing.—Data from each mode were independently analyzed using Progenesis QI software v2.3 (Nonlinear Dynamics). Metabolic features from blanks and that didn't show sufficient linearity upon dilution were discarded. Only metabolic features present in >33% of the samples in each group were kept for further analysis and missing values were imputed by drawing from a random distribution of small values in the corresponding sample[125].

Metabolic feature annotation.—Annotation confidence levels for each metabolite were provided following the Metabolomics Standards Initiative (MSI) confidence scheme. Peak annotation was first performed by matching experimental m/z, retention time and MS/MS spectra to an in-house library of analytical-grade standards (Level 1).

Remaining peaks were identified by matching experimental m/z and fragmentation spectra to publicly available databases including HMDB (http://www.hmdb.ca/), MoNA (http://mona.fiehnlab.ucdavis.edu/) and MassBank (http://www.massbank.jp/) using the R package 'MetID' (v0.2.0)[126] (Level 2). Briefly, metabolic feature tables from Progenesis QI were matched to fragmentation spectra with a m/z and a retention time window of ±15 ppm and ±30 s (HILIC) and ± 20 s (RPLC), respectively. When multiple MS/MS spectra match a single metabolic feature, all matched MS/MS spectra were used for the identification. Next, MS1 and MS2 pairs were searched against public databases and a similarity score was calculated using the forward dot–product algorithm which takes into account both fragments and intensities. Metabolites were reported if the similarity score was above 0.4. Level 3 corresponds to unknown metabolites.

Targeted lipidomics with the Lipidyzer platform.

Data acquisition.—Lipid extracts were analyzed using the Lipidyzer platform that comprises a 5500 QTRAP System equipped with a SelexION differential mobility spectrometry (DMS) interface (SCIEX) and a high flow LC-30AD solvent delivery unit (Shimazdu). A full description of the method is available elsewhere[123]. Briefly, the lipid molecular species were identified and quantified using multiple reaction monitoring (MRM) and positive/negative switching. Two acquisition methods were employed covering 10 lipid classes; method 1 had SelexION voltages turned on, while method 2 had SelexION voltages turned off. Lipidyzer data were reported by the Lipidomics Workflow Manager (LWM) v1.0.5.0 software, which calculates concentration in nmol/g for each detected lipid as average intensity of the analyte MRM/average intensity of the most structurally similar internal standard MRM multiplied by its concentration. Data quality was ensured by (i) tuning the DMS compensation voltages using a set of lipid standards (SCIEX #5040141) after each cleaning, more than 24 hours of idling or 3 days of consecutive use, (ii) performing a quick system suitability test (QSST) (SCIEX #50407) before each batch to ensure acceptable limit of detection for each lipid class, iii) sample randomization for lipid extraction and data acquisition, and iv) triplicate injection of lipids extracted from a reference plasma sample (SCIEX #4386703) at the beginning of the batch.

Data pre-processing.—Lipids detected in less than 66% of the samples in each group were discarded and missing values were imputed in each class by drawing from a random distribution of small values in the corresponding sample[125].

Differential analysis of metabolomics and lipidomics data

Metabolomics and lipidomics datasets were first normalized to the total protein content as determined by BCA assay (Pierce #23225) to account for differential starting material quantity. Then, Variance Stabilizing Normalization was applied to the data using 'limma' 3.42.2, as recommended by previous studies[127, 128]. Differential analysis for metabolomic or lipidomic features was performed using 'limma' in R. Features with a false discovery rate (FDR) < 5% were considered statistically significant.

For analysis of the lipidomics data by lipid class (Extended Data Figure 1; Supplementary Table S1F), lipids were summarized by class after BCA and VSN corrections. To determine

regulation at the class level, because of the small number of analyzed classes, a basic linear model approach was used through base R 'lm' function, and FDR correction was applied using the base R 'p.adjust' function. Lipid classes with a false discovery rate (FDR) < 5% were considered statistically significant.

Functional enrichment analysis for metabolomics

Since only 1 metabolite was significantly regulated with aging, we focused on analyzing differentially regulated metabolite sets with respect to sex. To analyze the directional regulation of metabolic pathways from untargeted metabolomics, we used R package 'MetaboAnalystR' 2.0.4[129] to perform Phenotype Set Enrichment analysis (PSEA)[130] of KEGG metabolic pathways. Using the 'mummichog' method[131], we provided an input table of metabolic peaks represented by mass over charge ratios (m/z) and retention time, limma-derived p-value and t-scores, and analysis mode (negative or positive ion) to have maximum sensitivity for the functional enrichment analysis of untargeted metabolomic data. All significant gene sets (FDR < 5%) are reported in Supplementary Table S4F.

Integrated functional enrichment analysis for RNA-seq and metabolomics using IMPaLA

Based on the differential analyses results in RNA-seq and metabolomics, we focused on analyzing differentially regulated genes and metabolites with respect to sex. To provide an integrated view of RNA-seq and metabolomics results, we took advantage of the IMPaLA paradigm[132]. We used the IMPaLA v12 web interface (http://impala.molgen.mpg.de/), which evaluates overrepresentation of genes and metabolites across 5055 annotated pathways from 12 databases, with default parameters. For the joint analysis, we used genes with FDR < 5% with respect to biological sex, using gene symbols as input IDs. For metabolic features, we selected only the manually validated species (Levels 1 and 2) with FDR < 5% with respect to biological sex. Finally, we also selected lipid species FDR < 5% with respect to biological sex. Importantly, we used HMDB IDs as input IDs for the metabolomic/lipidomic side of the analysis, thus analyzing only features with corresponding HMDB IDs. Joint analysis of significant features with a male bias, or, separately, those with female bias, were uploaded separately to the server (server access on 06–30-2020). All pathways with an overall combined FDR < 5% are reported in Supplementary Table S4H.

Functional enrichment analysis for lipidomics

Since there was no significant difference in lipid composition with aging, we focused on analyzing differentially regulated lipid sets with respect to sex. The Lipid Ontology (LION) website was used to perform functional enrichment analysis of lipids[133]. Lipid features with FDR < 5% with a male or female bias were uploaded to the server (access on 03–24-2020). For ease of reading, only the 10 most significant pathways with male and with female bias are shown in Figure 3f. All significant LION terms are reported in Supplementary Table S4G.

Neutrophil ATAC-seq library generation

An independent cohort of C57BL/6Nia mice was used to assess age- and sex-related differences in chromatin architecture using ATAC-seq. To assay potential differences in the

chromatin landscape of mouse bone marrow neutrophils across age and sex, we used the omni-ATAC protocol starting from 50,000 MACS-purified cells[134]. Libraries were quality controlled on the Agilent Bioanalyzer 2100 platform at the USC Genome Core before pooling. Libraries were multiplexed and sequenced on the Illumina HiSeq-Xten platform as paired-end 150bp reads at the Novogene Corporation (USA).

ATAC-seq preprocessing pipeline

Paired-end ATAC-seq reads were adapter-trimmed using NGmerge0.2[135], which clips overhanging reads in a sequence-independent fashion and has been recommended for use in ATAC-seq preprocessing. Trimmed paired-end were mapped to the mm10 genome build using bowtie2 (2.2.6)[136]. After alignment, PCR duplicates were removed using the 'rmdup' function of samtools (1.5). To minimize analytical artifacts from uneven sequencing depth between biological samples/libraries, libraries were randomly downsampled to the same depth for downstream analyses using PicardTools (2.20.3) or samtools (1.5). We used the peak finding function of HOMER (4.11) to identify ATAC-seq accessible regions[137].

Differential accessibility analysis with ATAC-seq

We extracted a normalized read count matrix from our the downsampled bam files over merged HOMER regions using R package 'Diffbind' 2.14 [138]. We used this extracted matrix for downstream analyses. Because of sample-to-sample variability, we used surrogate variable analysis [116] to estimate and correct for experimental noise, similar to the RNA-seq analysis. R package 'sva' 3.34 was used to estimate surrogate variables, and the 'removeBatchEffect' function from 'limma' 3.42.2 was used to regress out the effects of surrogate variables, PCR duplicate content and variation in reads mapping to peaks according to Diffbind (Fraction of reads in peaks). The 'DESeq2' R package (1.26.0) was used for further processing of ATAC-seq data. Regions with a false discovery rate < 5% were considered statistically significant.

Functional enrichment analysis of differentially accessible regions from ATAC-seq

We used the significantly differentially accessible peaks identified by DESeq2 at FDR < 5% to analyze functional enrichments linked to these regions. For this purpose, we leveraged the 'GREAT' 4.0.4 tool[139], a tool specifically optimized to identify functional enrichment starting from genomic regions. We used all ATAC-seq accessible regions as the background for enrichment. All other options were left to default parameters. Results were exported as 'tsv' and processed in R to filter significant regions at FDR < 5%. Filtered results are reported in Supplementary Tables S3F and S4I.

Chromatin architecture analysis from ATAC-seq datasets

To analyze the underlying chromatin architecture differences between neutrophils isolated from different biological groups, we used the NucleoATAC v0.3.4 software[68]. Since NucleoATAC requires high sequencing depth to reliably measure nucleosome profiles, we pooled depth-matched reads from each biological group to attain this depth as recommended by the authors of the software [68]. We extracted similar metrics from the NucleoATAC output to what was described in previous studies using this software to investigate chromatin

architecture[140]. All comparisons between groups were tested for statistical significance using two-tailed Wilcoxon rank-sum test (non-parametric test).

Repetitive element transcription analysis

To evaluate potential differential regulation of transposable elements, we used the 'analyzeRepeats.pl' functionality of the HOMER software to count STAR-mapped reads over repetitive elements[137]. To allow for whole library normalization, reads mapping over transcript were also counted using the same HOMER script. Read counts were imported into R to estimate differential repeat expression using the 'DESeq2' (1.26.0) R package[117].

Neutrophil NETosis assay

We used a flow-cytometry based NETosis assay protocol using extracellularized DNA staining by SYTOX Green to quantify cells undergoing NETosis, adapted from a flow cytometry-based protocol[141] and a 96-well plate plate-reader protocol[142], both with neutrophils in suspension. Briefly, MACS-purified neutrophils were resuspended in a concentration of 2×10^6 cells/mL in neutrophil culture medium (RPMI 1640 without phenol red [Hyclone], supplemented with 1% Pennicilin/Streptomycin [Corning] and 0.1% BSA [Akron Biotechnology]). We then used 1×10^6 cells, aliquoted into sterile microcentrifuge tubes, one per starting biological sample. SYTOX green (ThermoFisher Scientific # S7020) was added to each sample to a final concentration of 200nM. Neutrophil media supplemented with DMSO [Vehicle] or 50nM Phorbol 12-myristate 13-acetate [PMA] (Sigma # P1565) was added to each tube. Tubes were slowly inverted three times to mix. Then, 2×10^5 cells were seeded in technical quadruplicates in wells of a sterile black 96-well plate [Greiner Bio-One] and incubated in a humidified incubator with 5% CO_2 at 37°C for 2 hours. The fraction of cells positive for SYTOX Green in each well was quantified using the MACSQuant10 and analyzed using Flowlogic V7. To account for differences in basal levels of NETosis across samples, NETosis was expressed as induction of NETosis: (median of PMA technical quadruplicates) / (median of DMSO technical quadruplicates). The raw cytometry dataset was deposited to Figshare (doi.org/10.6084/m9.figshare.14043923.v1).

TNFα-primed NETosis analysis

To compare our results with previously published results on NETosis in aged neutrophils[13, 14] [which were obtained with direct TNFα priming[13] or in conditions known to mimic TNFα priming[14] (*i.e.* thioglycolate elicitation of peritoneal neutrophils[71])], we also performed NETosis analysis in primed conditions, using a slightly modified protocol from above to include a priming step. Specifically, the MACS-purified neutrophils cells were resuspended in neutrophil culture medium and first pre-warmed after isolation in a humidified incubator with 5% CO2 at 37°C for 15 minutes. Then, 2×10^6 cells were aliquoted into a sterile microcentrifuge tube, and primed with 10ng/mL mouse TNFα (PeProTech # 315–01A) in a humidified incubator with 5% CO2 at 37°C for 15 minutes. Cells were then further aliquoted, supplemented with SYTOX green, DMSO/PMA, incubated and analyzed as above. The raw cytometry dataset was deposited to Figshare (doi.org/10.6084/m9.figshare.14043923.v1).

Feature extraction for machine-learning analysis

For each significantly age-regulated or sex-dimorphic gene in neutrophils according to DEseq2 (FDR < 5%), we extracted a number of features associated to that gene. First, we took advantage of our ATAC-seq data to evaluate the chromatin architecture of neutrophils (see above). For each gene, we extracted (i) the average promoter accessibility by ATAC-seq in FPKM across all 4 conditions (promoters were defined as −500bp;+150bp with regards to annotated transcriptional start sites in mm10 build according to HOMER), as well as (ii) the average $\log_2$(Fold Change) in accessibility between old and young neutrophils (age-regulation models) or the average $\log_2$(Fold Change) in accessibility between female and male neutrophils (sex-dimorphism models). Second, we took advantage of gene sets coverage known of predicted targets of transcriptions factors: ChEA, ENCODE, JASPAR and GEO TF perturbation information from the Harmonizome database[122] and transcriptional targets of FOXO transcription factors from GEO experiments compiled in our previous study[18]. To reduce extraneous features, we engineered a TF target feature following these steps: (i) TF targets were summarized from all putative sources, (ii) only TFs with evidence of expression in primary neutrophils according to RNA-seq were retained as features, and (iii) only TFs with at least 25 targets across significant age-related genes (age-regulation models) or sex-dimorphic genes (sex-dimorphism models) were retained. This process yielded 357 (age-regulation models) and 249 (sex-dimorphism models) TF target sets used as features for model training. Finally, we included several DNA sequence features to each gene: the percentage of CG nucleotide and the percentage of CpG dinucleotide in promoters and exons, computed using HOMER. To note, HOMER was only able to provide information for 3,421 of the 3,653 genes with significant age regulation, and 1,636 of the 1,734 genes with significant sex-dimorphic regulation. Finally, to determine whether location of the gene on autosomes *vs.* chromosomes was a key predictive factor for sex-dimorphic gene expression, we also included for the sex-dimorphic gene expression models a feature encoding whether the gene is located on autosomes or sex chromosomes (X or Y).

Machine-learning analysis for age-regulated or sex-dimorphic genes

We trained machine-learning classification models for 2 questions: (i) models for age-regulated gene expression, and (ii) models for sex-dimorphic gene expression. For (i), age-regulation machine-learning models were built to learn whether up- or down-regulated genes could be discriminated using genomic features and predict potential master regulators. For (ii), sex-dimorphism machine-learning models were built to learn whether female and male biased genes could be discriminated using genomic features and predict potential master regulators.

In both cases, we built classification models using 7 classification algorithms as implemented through R package ‘caret’ (caret 6.0–86). Auxiliary R packages were used with ‘caret’ to implement neural networks (NNET; ‘nnet’ 7.3–13), random forests (RF; ‘randomForest’ 4.6–14), gradient boosting (GBM; ‘gbm’ 2.1.5), radial kernel support vector machines (SVM; kernlab 0.9–29), sparse Linear Discriminant Analysis (LDA; ‘sparseLDA’ 0.1–9), conditional inference Trees (cTree; ‘party’ 1.3–4), Regularized Logistic Regression (LogReg; ‘LiblineaR’ 2.10–8). ‘Caret’ was allowed to optimize final model parameters

on the training data using 10-fold cross validation. Accuracies, sensitivities, specificities and AUC (using package 'pROC' 1.16.2) for all trained classifiers were estimated using a test set of randomly held out 1/3 of the data (not used in the training phase) obtained using the 'createDataPartition' function. Feature importance estimation was only done using tree-based RF and GBM methods, since other algorithms do not natively allow for it. The feature importance was computed and scaled by 'caret' for the RF and GBM models.

Reanalysis of DIA proteomics data from human neutrophils

We obtained DIA proteomics results from the supplemental material of a recent study[97]. We used normalized expression values from the article's supplemental material and used the reported "donor-specific Spectronaut protein expression values" for further analysis. To exclude potential confounds linked to disease, we only used data from the 68 healthy donors [HD] and excluded the data from diseased patients. Since the article did not report the biological sex of donors, we used detected expression levels of DDX3Y, a Y-chromosome encoded protein, as a proxy for the likelihood of the sample belonging to a male donor. We then examined rank correlation statistics between protein expression of DDX3Y compared to that of human orthologs of top male-biased primary granules genes from our mouse RNA-seq data (*i.e.* ELANE, MPO, PRTN3 and CTSG). Significance of the Spearman rank correlation is reported.

Mouse sepsis model through intra-peritoneal LPS injection

Young adult (3–4 months) C57BL/6J mice were exposed to LPS, a pathogen-associated molecular pattern (PAMP) found in the cell-wall of Gram-negative bacteria, to elicit a sepsis-like response[96]. Briefly, mice were injected intra-peritoneally with 2μg of LPS per gram of body weight, using a sterile LPS stock (Sigma #L5293) diluted in PBS, and control animals were injected with sterile PBS[96]. Animals were monitored hourly for up to 6 hours after injection for the occurrence and severity of endotoxemia[96]. We did not observe gross differences in the state of female *vs.* male animals injected with LPS over the course of the experiment, although it is possible that such differences would have emerged at longer time-points. After euthanasia by CO_2 asphyxiation and cervical dislocation at 1, 3 and 6 hours post injection, blood was collected from the heart. A total of 80 animals across 3 independent experimental days were used (n = 8 animals per sex, age and time group for LPS injections; n = 5 animals per sex, age and time group for control PBS injections). To obtain serum for downstream analysis, the blood was left to clot for ≥1 hour at room temperature in MiniCollect Serum SeparatorTubes (Greiner Bio-One). The serum was then separated from the clot using centrifugation at 2,000g for 10 minutes, and frozen at −80°C until further use.

Quantification of serum neutrophil elastase (ELANE) by ELISA

Quantitative evaluation of circulating ELANE levels was performed from serum. ELISA quantification of serum ELANE levels was performed using Abcam's Mouse Neutrophil Elastase SimpleStep ELISA Kit (ab252356) according to the manufacturer's instructions. Technical replicates from the same sample were averaged as one value before statistical analysis and plotting.

Statistics and reproducibility

All statistical analyses were conducted using R version 3.6.0–3.6.3. For all 'omic' analyses, results were corrected for multiple testing by the use of False Discovery Rate [FDR] significance correction. All statistical analyses were performed as specified in the figure legends and in the corresponding methods section. We used non-parametric statistical tests whenever possible to avoid assuming normality of data distributions. No statistical methods were used to predetermine sample size, since effect sizes and variance were not known *a priori*. No data passing quality control checks were excluded from the analyses. All 'omic' samples were performed on independent biological samples, usually from one cohort of animals to minimize known issues linked to batch effects in such analyses[143]. As one exception, RNA-seq of bone marrow neutrophils was independently replicated on a smaller cohort, since neutrophils are known to be RNA-poor, which could add more than usual biological variability (Extended Data Figure 2). With the exception of a test of the heterogeneity flow cytometry panel on bone marrow cells (used to validate c-kit staining; Extended Data Figure 4b; Supplementary Table S2B), all other experiments were performed on animals from at least 2 independent cohorts.

For each experiment, animals were processed in an alternating/snaking order rather than in large homogeneous groups to minimize group, batch and circadian effects. For observational aging studies, no randomization is possible since groups are biologically determined. For LPS injection experiments, animals were randomly allocated to the PBS or LPS group for a euthanasia time point, on a cage-level basis (*i.e.* animals from the same cage randomly attributed to LPS vs. PBS injections; for each cohort, co-housed animals were used for the same time point; cages attributed to a specific euthanasia time point randomly). This process was performed independently for each of the 3 cohorts for LPS-induced endotoxemia. Blinding was not relevant to the studies conducted here, as the data are collected by automated systems (*i.e.* sequencing, mass-spectrometry, flow cytometry) or in numeric form (*i.e.* ImageJ quantification of Western Blot bands, ELISA absorbance values), which cannot be influenced by subjectivity from the experimenter.

Data Availability

Sequencing data has been submitted to the Sequence Read Archive (SRA) accessible through BioProject PRJNA630663. Untargeted metabolomics data was uploaded to metabolomics workbench DataTrack ID 2089. The lipidomics data is available as Supplemental Table S7 and was deposited in Figshare (https://doi.org/10.6084/m9.figshare.14524278). Raw flow cytometry data was deposited to Figshare (doi.org/10.6084/m9.figshare.14043938.v1, doi.org/10.6084/m9.figshare.14043932.v1, doi.org/10.6084/m9.figshare.14043929.v1, doi.org/10.6084/m9.figshare.14043926.v1, and doi.org/10.6084/m9.figshare.14043923.v1). Western Blot raw and cropped images have been deposited to Figshare (https://doi.org/10.6084/m9.figshare.14154665).

We reanalyzed publicly available neutrophil RNA-seq data from GEO Datasets GSE1248296 (6 weeks-old mouse spleen neutrophil samples), and GSE145231 (human blood neutrophil samples), and human neutrophil DIA proteomics data (https://www.ncbi.nlm.nih.gov/pmc/articles/PMC6442368/bin/

141289_1_supp_251888_pjqfps.xlsx). Functional gene annotations were obtained from ENSEMBL Biomart (https://www.ensembl.org/biomart/martview/), the Molecular Signature Database (http://www.gsea-msigdb.org/gsea/msigdb/collections.jsp) and the Harmonizome (https://maayanlab.cloud/Harmonizome/download). Mass-spectrometry peaks were identified by matching experimental m/z and fragmentation spectra to publicly available databases including HMDB (http://www.hmdb.ca/), MoNA (http://mona.fiehnlab.ucdavis.edu/) and MassBank (http://www.massbank.jp/).

Code Availability

The analytical code is available on the Benayoun lab Github repository (https://github.com/BenayounLaboratory/Neutrophil_Omics_2020). All R code was run using R version 3.6.0–3.6.3.

Extended Data

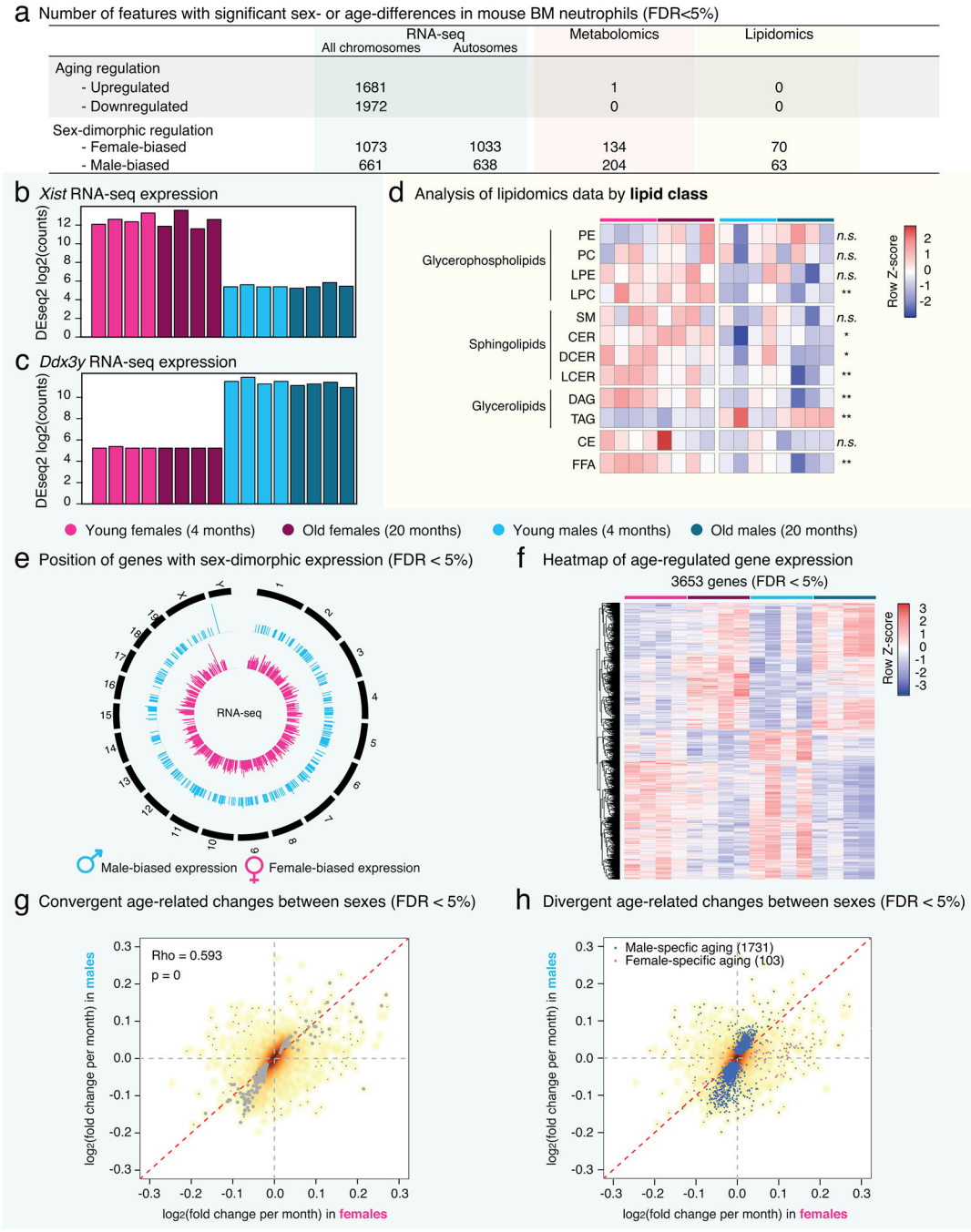

Extended Data Figure 1: A multi-omic analysis of primary mouse bone marrow neutrophils during aging and with respect to sex (continued).

(**a**) Table of significant "omic" features as a function of organismal age and sex in our datasets based on DEseq2 (RNA-seq) or limma (Metabolomics and lipidomics), at FDR < 5%. For the analysis of sex-dimorphism in gene expression, the number of significant genes located on autosomes (*i.e.* not on chromosomes X or Y) is also reported. (**b-c**) Barplot of DESeq2-normalized log2 counts for *Xist* (b) and *Ddx3y* (c), showing the expected pattern

between male and female samples, which acts as a quality check for our dataset. (**d**) Heatmap of lipidomic changes summarized by lipid classes. Significance of difference as a function of age or sex was evaluated using a linear model, and the significance of the sex coefficient (as reported by the R 'lm' function) is reported on the line of the heatmap. *: $p < 0.05$; ** : $p < 0.01$; n.s. : $p \geq 0.05$. See also Supplementary Table S1F. (**e**) Circular genome plot of the positions of genes with significant sex-biased gene expression in neutrophils (FDR < 5%). (**f**) Heatmap of significant age-regulated genes (DESeq2 FDR < 5%). (**g-h**) Correlation plot of age-related gene expression change according to DESeq2 in female *vs.* male neutrophils from RNA-seq, showing genes with (g) significant and concordant age-regulation in both sexes at FDR 5%, or (h) genes with divergent age-regulation between sexes (FDR < 5% in one sex, and FDR >15% in the other). Spearman Rank correlation (Rho), and significance of this correlation are reported in (g). Importantly, age was inputted into the DEseq2 model as a continuous numerical variable (expressed in months), which yields fold change values per month of life.

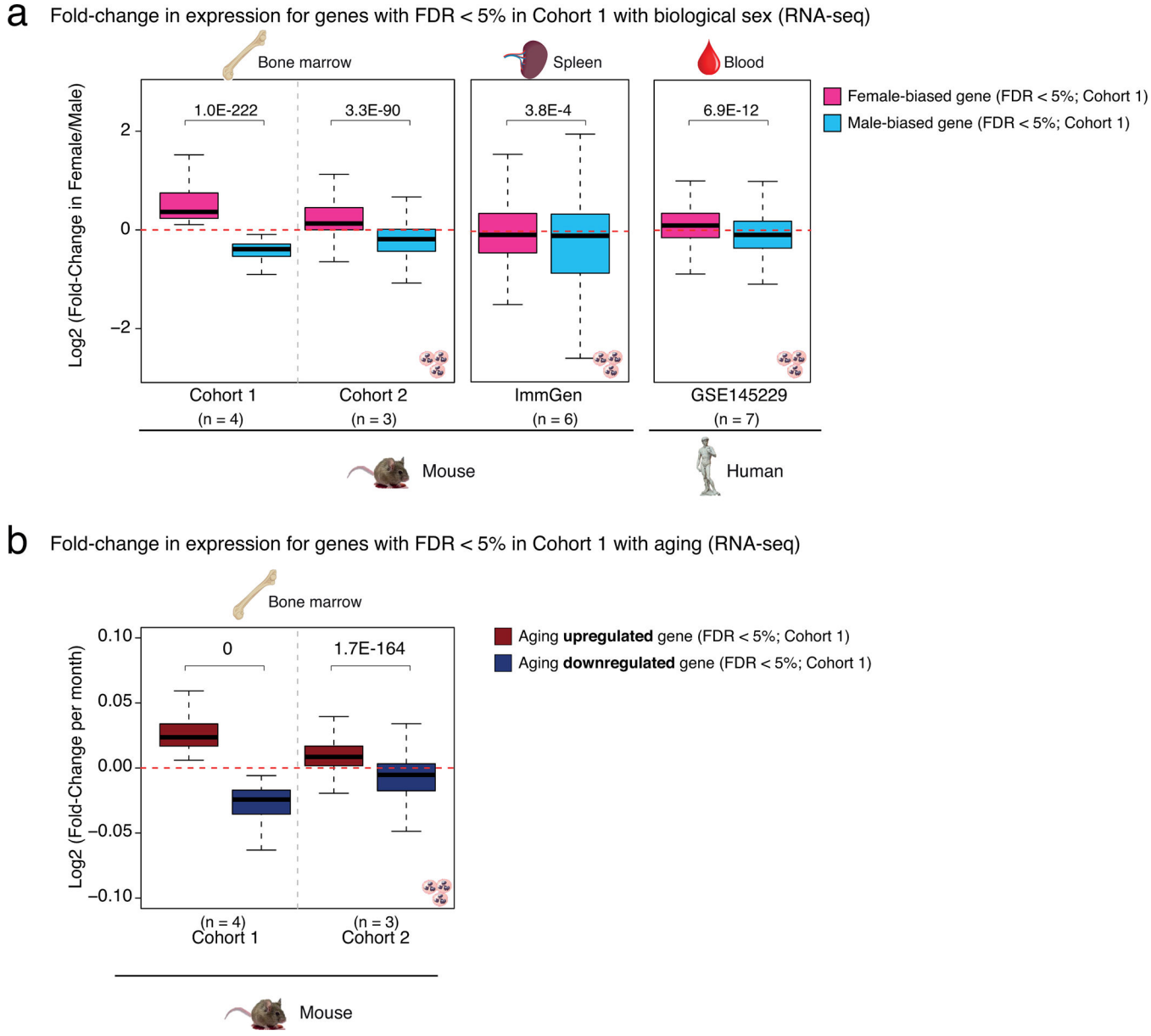

Extended Data Figure 2: Comparison to other neutrophil RNA-seq datasets.

(**a**) DESeq2 normalized $\log_2$ fold changes as a function of biological sex for differentially expressed mouse genes from our original cohort (FDR <5%) (and their human orthologs) across datasets [see Methods]. The original mouse bone marrow neutrophil cohort data are plotted for comparison as the leftmost panel. On the right are plotted corresponding $\log_2$ fold change values from our own smaller replication cohort of mouse bone marrow neutrophils (n = 3 per group), from mouse spleen neutrophils from ImmGen[23] and a human blood neutrophil cohort[25]. P-values were calculated using a two-sided Wilcoxon test between female-biased and male-biased genes from our original cohort across new datasets, to test the robustness of such differences between our original cohort and new datasets. (**b**) DESeq2 normalized $\log_2$ fold changes per month during aging for differentially age-regulated mouse genes from our original cohort (FDR <5%). The original mouse bone marrow neutrophil

cohort data are plotted for comparison as the leftmost panel. On the right are plotted corresponding $\log_2$ fold change values from our own smaller replication cohort of mouse bone marrow neutrophils (n = 3 per group). P-values were calculated using a two-sided Wilcoxon test between upregulated *vs.* downregulated genes, to test the robustness of such differences between our original cohort $\log_2$ fold changes and a new dataset. The center line represents the sample median, the box limits consist of the 25th and 75th percentiles, the whiskers span 1.5x the interquartile range, and each RNA-seq sample is represented by a point on the graph.

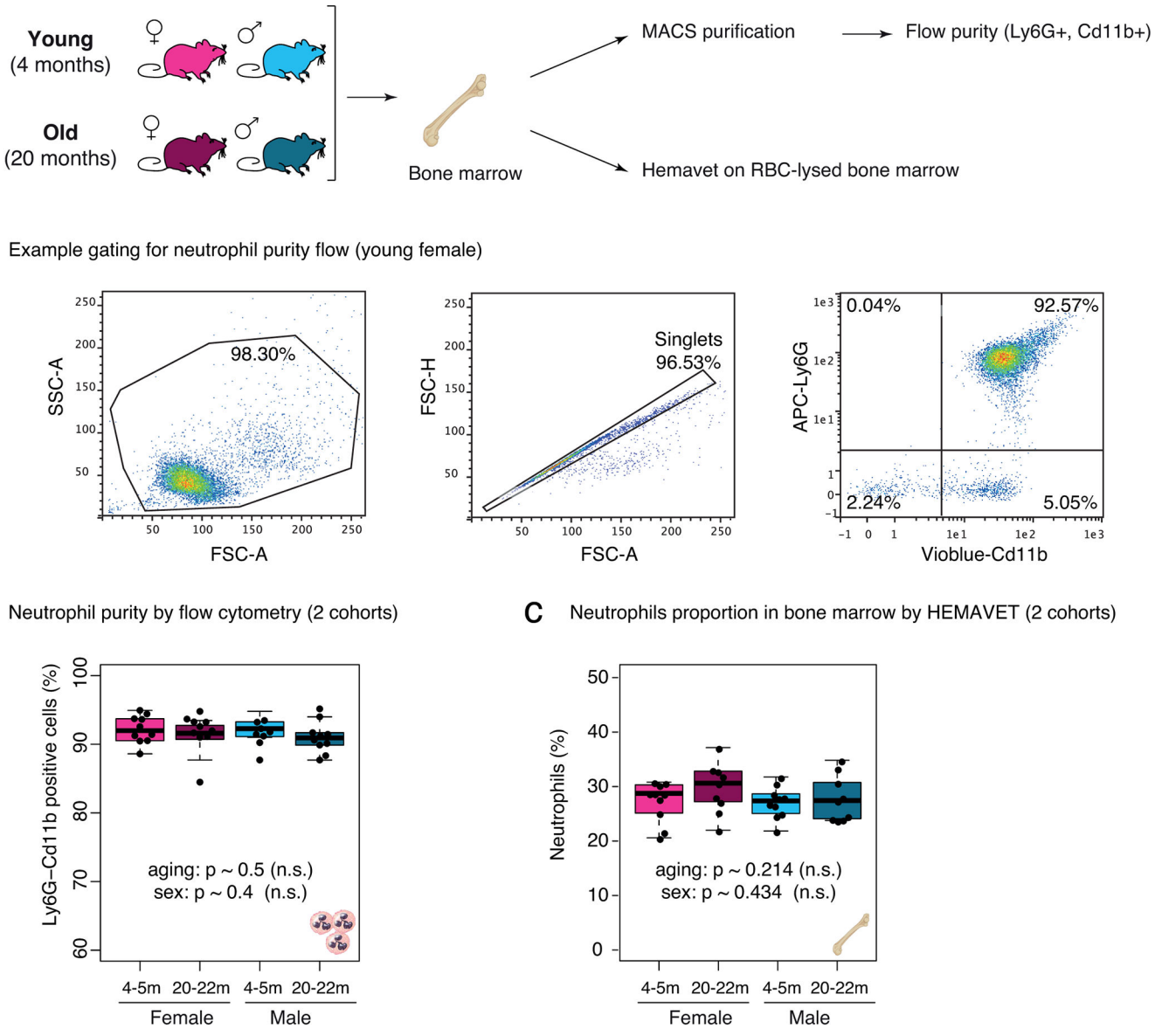

Extended Data Figure 3: Bone marrow neutrophil purity is not impacted by animal sex or organismal age.

(**a**) Representative flow cytometry gating strategy of bone-marrow neutrophils purified using MACS from a young female mouse. Neutrophils are expected to be double positive for

Cd11b and Ly6G. (**b**) Neutrophil purity from 2 independent cohorts of aging male vs. female mice (n = 8 for old females, and n = 10 per group for all other groups), determined as the Cd11b+ Ly6G+ population. (**c**) Proportion of neutrophils among bone marrow nucleated cells according to the Hemavet 950FS from 2 independent cohorts of aging male vs. female mice (n = 9 for old females, and n = 10 per group for all other groups). Statistical analysis for (b) and (c) derived from a linear modeling analysis with sex and age as covariates, similar to our "omic" analysis models, with significance of coefficients as reported by the R 'lm' function. The center line represents the sample median, the box limits consist of the 25th and 75th percentiles, the whiskers span 1.5x the interquartile range, and each RNA-seq sample is represented by a point on the graph.

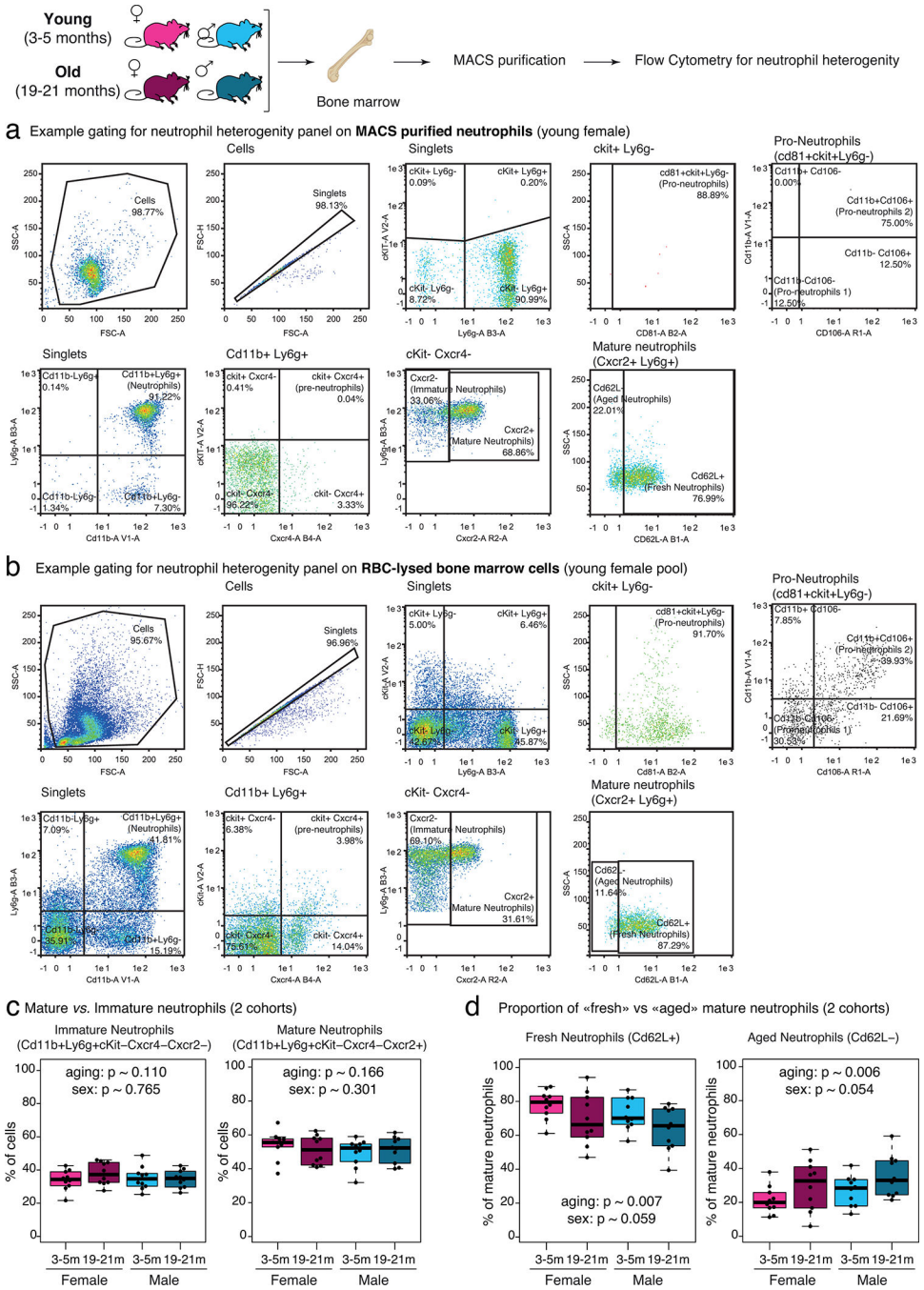

Extended Data Figure 4: Analysis of MACS-purified bone marrow neutrophil heterogeneity.

(**a**) Representative flow cytometry gating strategy of bone-marrow neutrophils purified using MACS from a young female mouse. Populations were defined according to previously published markers[136, 137, 138]. Specifically, among live cell singlets, pro-neutrophils were defined as c-Kit^{+}Ly6g^{-}Cd81^{+}, with subpopulation of pro-neutrophil 1 defined as c-Kit^{+}Ly6G^{-}Cd81^{+}CD11b^{-}CD106^{-} and pro-neutrophils 2 as c-Kit^{+}Ly6G^{-}Cd81^{+}CD11b^{+}CD106^{+}. Pre-neutrophils were defined as Cd11b^{+}Ly6G^{+}c-Kit^{+}Cxcr4^{+} cells. Immature neutrophils were defined as CD11b^{+}Ly6G^{+}c-Kit^{-}Cxcr4^{-}Cxcr2^{-}

cells, and mature neutrophils as $CD11b^{+}Ly6G^{+}c\text{-}Kit^{-}Cxcr4^{-}Cxcr2^{+}$. Fresh *vs.* "aged" subsets of mature neutrophils were defined respectively as $CD11b^{+}Ly6G^{+}c\text{-}Kit^{-}Cxcr4^{-}Cxcr2^{+}CD62L^{+}$ *vs.* $CD11b^{+}Ly6G^{+}c\text{-}Kit^{-}Cxcr4^{-}Cxcr2^{+}CD62L^{-}$ cells. The gate from which cells are plotted is indicated above each flow cytometry plot. (**b**) Representative flow cytometry gating strategy of RBC-lysed bone marrow cells from a young female mouse. The gate from which cells are plotted is indicated above each flow cytometry plot. This analysis was run as a control for the presence/abundance of $cKit^{+}$ cells, as MACS-purified cells had extremely low numbers of these cells. (**c**) Amounts of immature (left) *vs.* mature (right) neutrophil among all MACS-purified cells from 2 independent cohorts of aging male *vs.* female mice (n = 10 per group). (**d**) Proportion of "fresh" vs. "aged" neutrophils among mature neutrophils from 2 independent cohorts of aging male *vs.* female mice (n = 10 per group). Statistical analysis for (c) and (d) derived from a linear modeling analysis with sex and age as covariates, similar to our "omic" analysis models, with significance of coefficients as reported by the R 'lm' function. The center line represents the sample median, the box limits consist of the 25th and 75th percentiles, the whiskers span 1.5x the interquartile range, and each RNA-seq sample is represented by a point on the graph. Also see Supplementary Table S2 for quantifications of all populations.

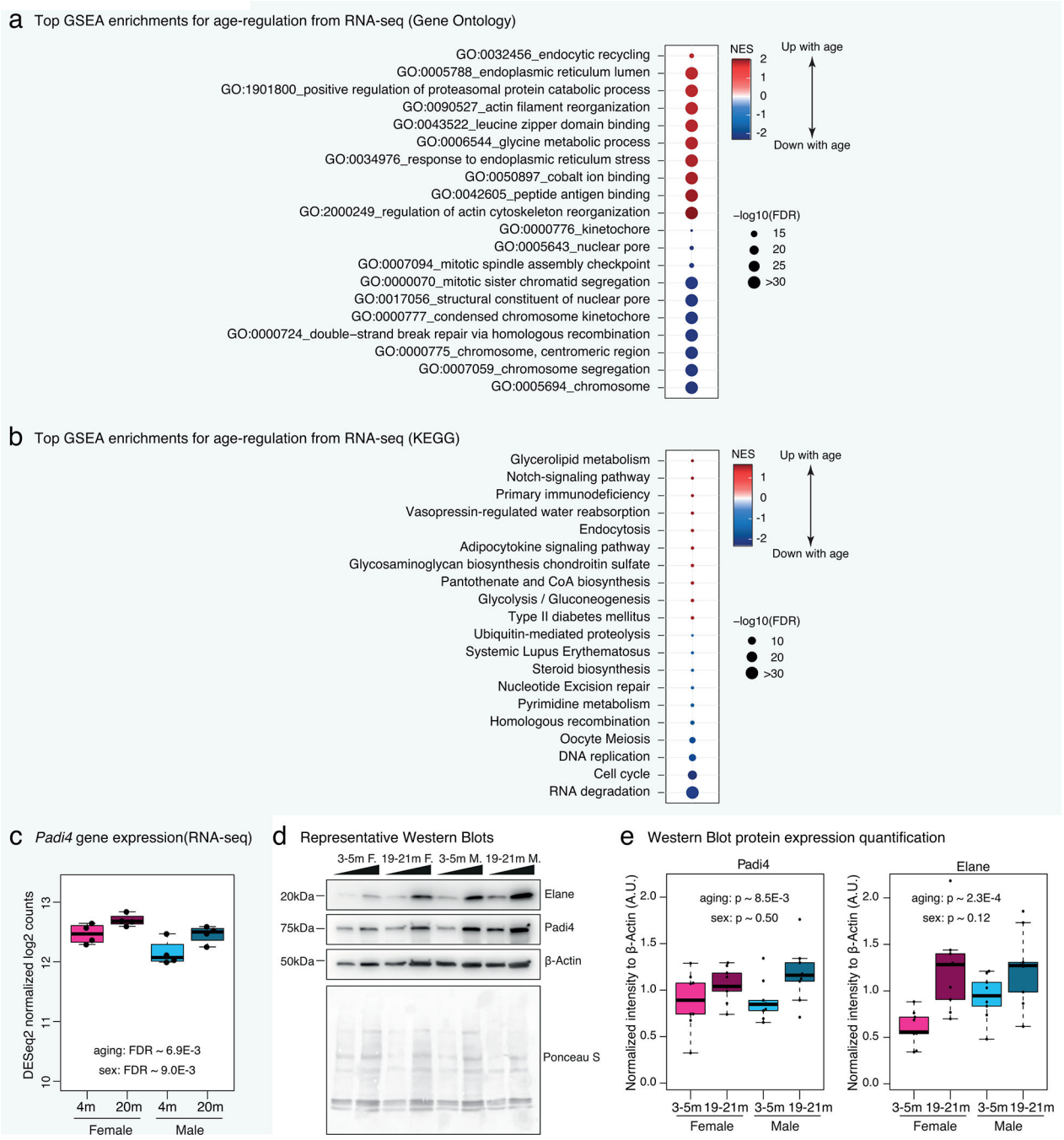

Extended Data Figure 5: Regulated pathways in bone marrow neutrophils during aging reveals downregulation of chromatin-related pathways (continued).

(**a-b**) Top enriched gene sets from Gene Ontology (a) and KEGG (b) using GSEA for differential RNA expression. Only the top 10 most up- and top 10 most downregulated gene sets are plotted for readability. Full lists and statistics available in Supplementary Table S2. Shown pathways with FDR < 5%. (**c**) Boxplot of *Padi4* transcriptional levels from RNA-seq. Significance: DESeq2 FDR values for regulation as a function of aging or biological sex. The center line represents the sample median, the box limits consist of the

25th and 75th percentiles, the whiskers span 1.5x the interquartile range, and each RNA-seq sample is represented by a point on the graph (n = 4 RNA-seq samples per group). (**d**) Representative Western Blot images for primary bone marrow neutrophils for Elane, Padi4 and β-actin (loading control), as well as Ponceau S staining of PVDF blotting membrane. The membrane was cut along predicted molecular weights, and each strip was probed for each specific protein in that range. (**e**) Boxplot of quantification of Western Blot for Padi4 (left) and Elane (right) from primary bone marrow neutrophils. Data from 2 independent cohorts of aging male *vs.* female mice (n = 9 per group). Two concentrations of the same sample were loaded side by side for each biological sample. Statistical analysis derived from a linear modeling analysis with sex and age as covariates, similar to our "omic" analysis models, with significance of coefficients as reported by the R 'lm' function. The center line represents the sample median, the box limits consist of the 25th and 75th percentiles, the whiskers span 1.5x the interquartile range, and each RNA-seq sample is represented by a point on the graph. All uncropped western blot images and quantification data is been made available on Figshare (https://doi.org/10.6084/m9.figshare.14154665.v1). NES: Normalized Enrichment Score (for GSEA analysis). FDR: False Discovery Rate.

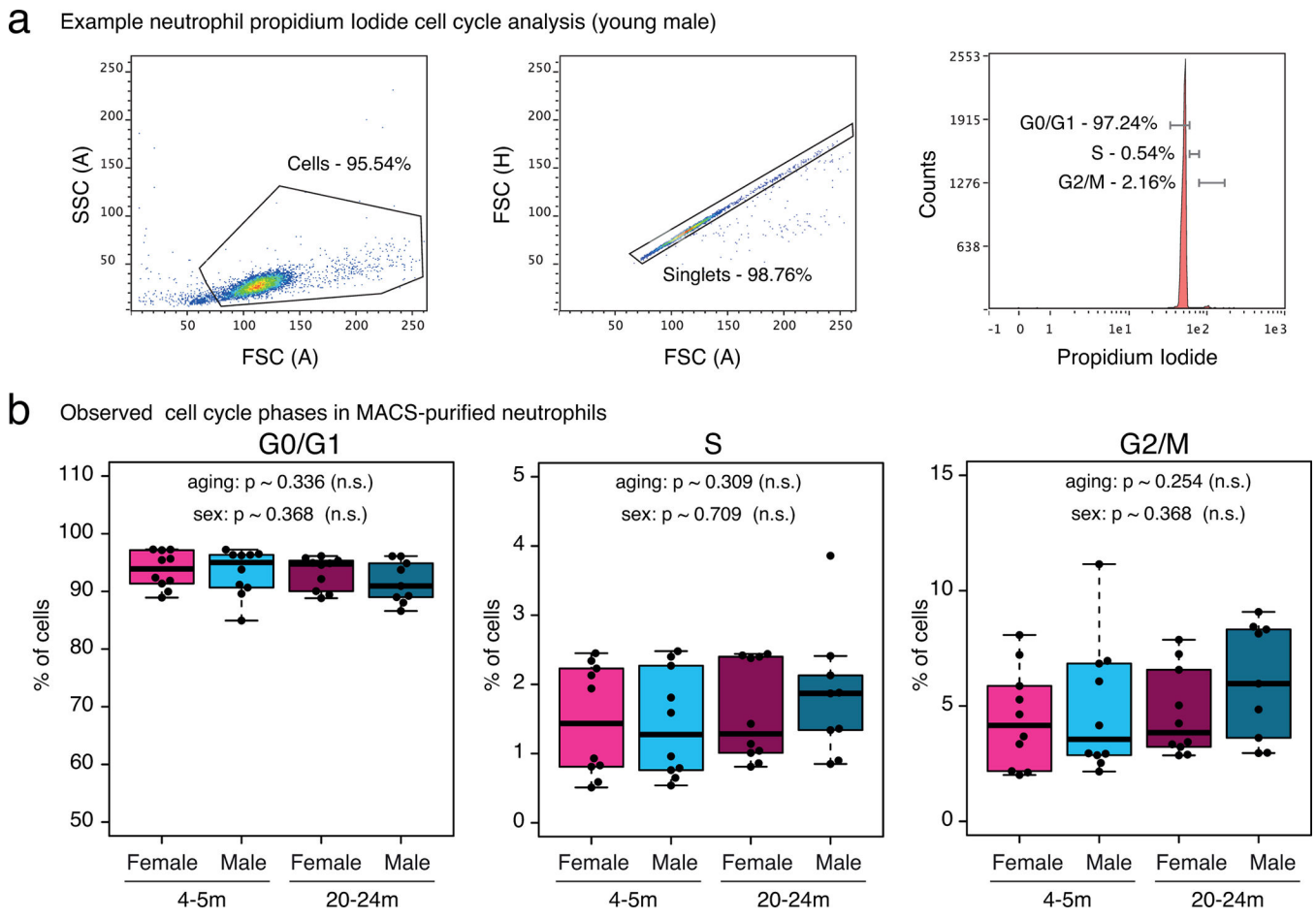

Extended Data Figure 6: The distribution of cell cycle phases of MACS-purified bone marrow neutrophil is not impacted by animal sex or organismal age.

(**a**) Representative flow cytometry gating strategy of bone-marrow neutrophils purified using MACS from a young male mouse stained using Propidium Iodide to assess cell-cycle phase based on DNA content. Neutrophils are expected to be largely post-mitotic. (**b**) Boxplots of MACS-purified bone marrow neutrophil cell cycle distribution (G0/G1, S or G2/M) from 2 independent cohorts of aging male *vs.* female mice (n = 9 for old males, and n = 10 per group for all other groups), determined by DNA content. The overwhelming majority of samples have > 90% cells in G0/G1, and there are no trends associated to organismal age or biological sex. Statistical analysis for (b) derived from a linear modeling analysis with sex and age as covariates, similar to our "omic" analysis models, with significance of coefficients as reported by the R 'lm' function. The center line represents the sample median, the box limits consist of the 25th and 75th percentiles, the whiskers span 1.5x the interquartile range, and each RNA-seq sample is represented by a point on the graph.

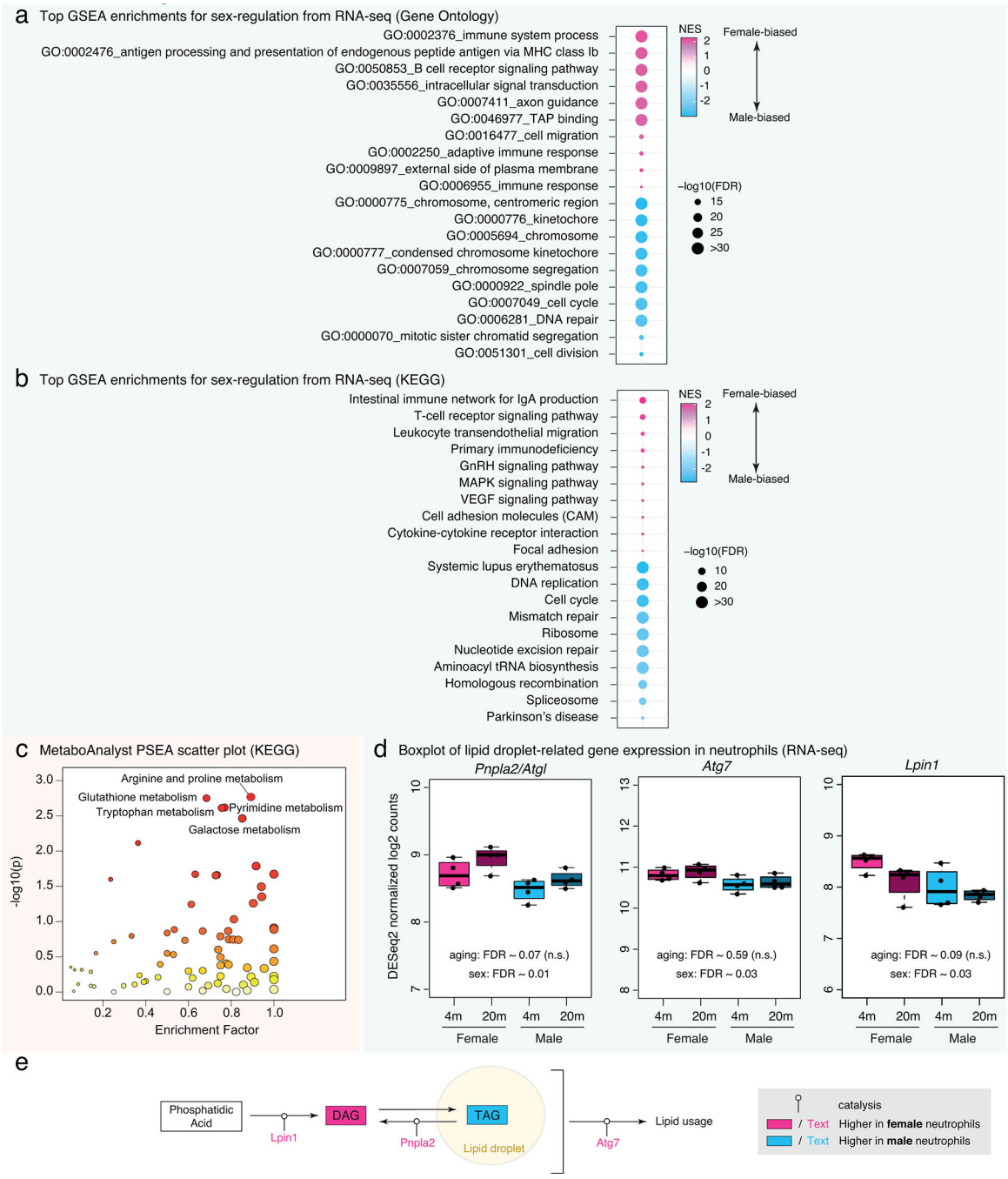

Extended Data Figure 7: Sex-dimorphic pathways in bone marrow neutrophils reveal differential regulation of chromatin-related pathways (continued).

(**a-b**) Top enriched gene sets from Gene Ontology (a) and KEGG (b) using GSEA for differential RNA expression as a function of sex. Only the top 10 most up- and top 10 most downregulated gene sets are plotted for readability. Full lists and statistics available in Supplementary Table S2. All shown pathways and genes such as FDR < 5%. (**c**) MetaboAnalyst PSEA scatterplot for KEGG pathways from metabolomics. NES: Normalized Enrichment Score (for GSEA analysis). FDR: False Discovery Rate. (**d**)

Boxplot of transcriptional levels from our RNA-seq for *Pnpla2/Atgl*, *Atg7* and *Lpin1*, which are sex-dimorphic lipid metabolism-related genes. The significance is derived from DESeq2, and we report the corresponding FDR values for regulation as a function of aging or biological sex. The center line represents the sample median, the box limits consist of the 25th and 75th percentiles, the whiskers span 1.5x the interquartile range, and each RNA-seq sample is represented by a point on the graph (n = 4 RNA-seq samples per group). (**e**) Summary scheme of discussed lipid usage in female vs. male neutrophils based on lipidomic and transcriptomic data. Catalyzed reactions are derived from Wikipathway WP3901 (Lipid droplet metabolism) and [37].

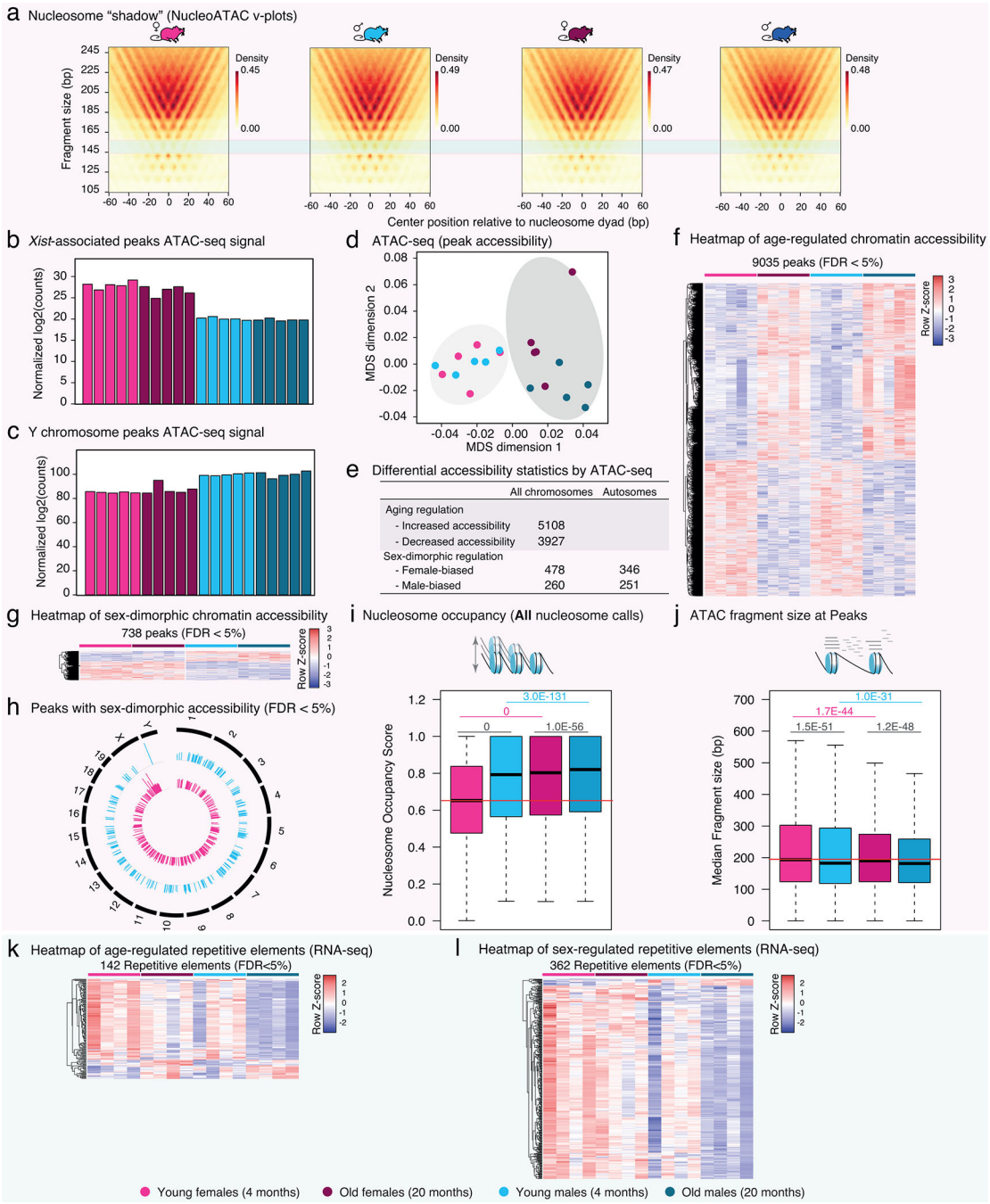

Extended Data Figure 8: ATAC-seq analysis reveals age- and sex-related differences in the chromatin architecture of bone marrow neutrophils (continued).

(**a**) NucleoATAC v-plots. The light green box overlay reveals a v-plot region where males have higher signal than females, regardless of age, suggesting differences in nucleosomal architecture.

(**b-c**) Barplot of DESeq2-normalized log2 counts at ATAC-seq peaks associated to *Xist* (b) or situated on the Y chromosome (c), showing the expected pattern between male and female samples. (**d**) Multidimensional Scaling analysis results of chromatin accessibility

from ATAC-seq. (**e**) Table of significantly differentially accessible ATAC-seq peaks as a function of organismal age and sex. The number of significant peaks located on autosomes (*i.e.* not on chromosomes X or Y) is also reported. (**f-g**) Heatmap of accessibility at peaks with significant age-regulated (f) or sex-dimorphic (g) change in accessibility (FDR < 5%). (**h**) Circular genome plot of the genomic positions of peaks with significant sex-bias in neutrophil ATAC-seq (FDR < 5%). (**i**) Boxplot of nucleosome occupancy as calculated by NucleoATAC for all called nucleosomes across groups. Also see Figure 4d. (**j**) Boxplot of median ATAC-seq fragment length at ATAC-seq peaks across experimental groups. The horizontal red line in panels (i,j) shows the median value in neutrophils from young females for ease of comparison. Significance in non-parametric two-sided Wilcoxon rank-sum tests are reported for panels (i,j). Black p-values represent differences between male *vs.* female neutrophils in each age group; pink (blue) p-values represent age-related differences in female (male) neutrophils. For boxplots in panels (i,j), the center line represents the sample median, the box limits consist of the 25th and 75th percentiles, the whiskers span 1.5x the interquartile range, for readability and consistent with practices in genomics, outliers are not shown on the graph although they are always taken into account for the statistics. (**k-l**) Heatmap of repetitive elements with significant age-regulated (k) or sex-dimorphic (l) change in transcription from RNA-seq (FDR < 5%).

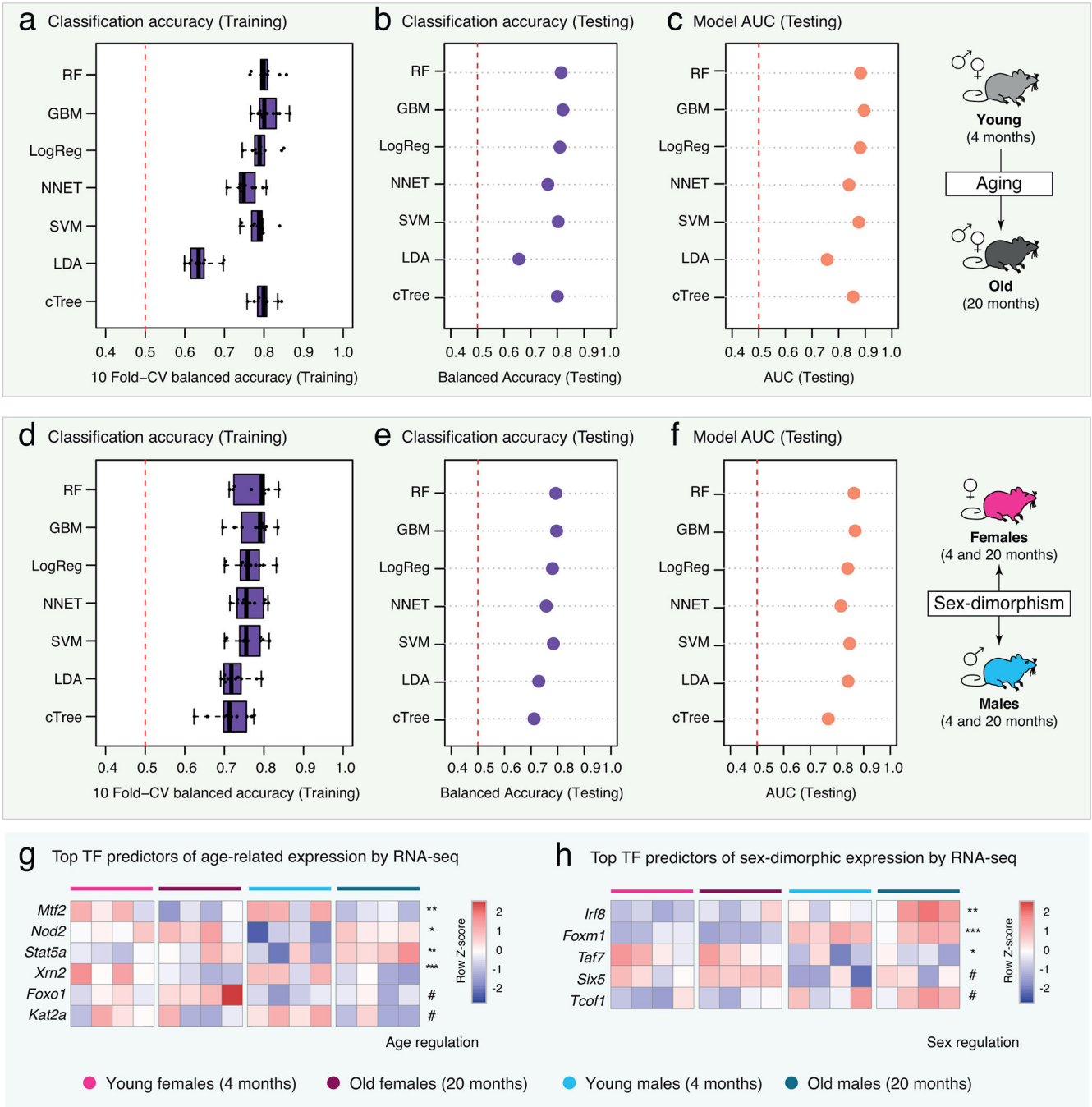

Extended Data Figure 9: Machine-learning analysis reveals that age-regulated and sex-dimorphic gene expression can be predicted by genomic and epigenomic features.

(**a-c**) Age-related machine-learning model performance metrics: balanced classification accuracy over the 10 cross-validation folds during model training (a), balanced classification accuracy on held-out testing data (b), and Area Under the Curve [AUC] on held-out testing data (c). Also see Supplementary Table S5A. (**d-f**) Sex-dimorphism machine-learning model performance metrics: balanced classification accuracy over the 10 cross-validation folds during model training (d), balanced classification accuracy on held-out testing data (e), and

Area Under the Curve [AUC] on held-out testing data (f). Also see Supplementary Table S5C. (**g-h**) Heatmap of RNA-seq expression level for top TF predictors in age-regulated (g) or sex-dimorphic (h) gene expression models with FDR < 10%. DESeq2 FDR is reported on each line, with # : FDR < 0.1; * : FDR < 0.05; ** : FDR < 0.01; *** : FDR < 0.001. FDR: False Discovery Rate. For boxplots in panels (**a,d**), the center line represents the sample median, the box limits consist of the 25th and 75th percentiles, the whiskers span 1.5x the interquartile range.

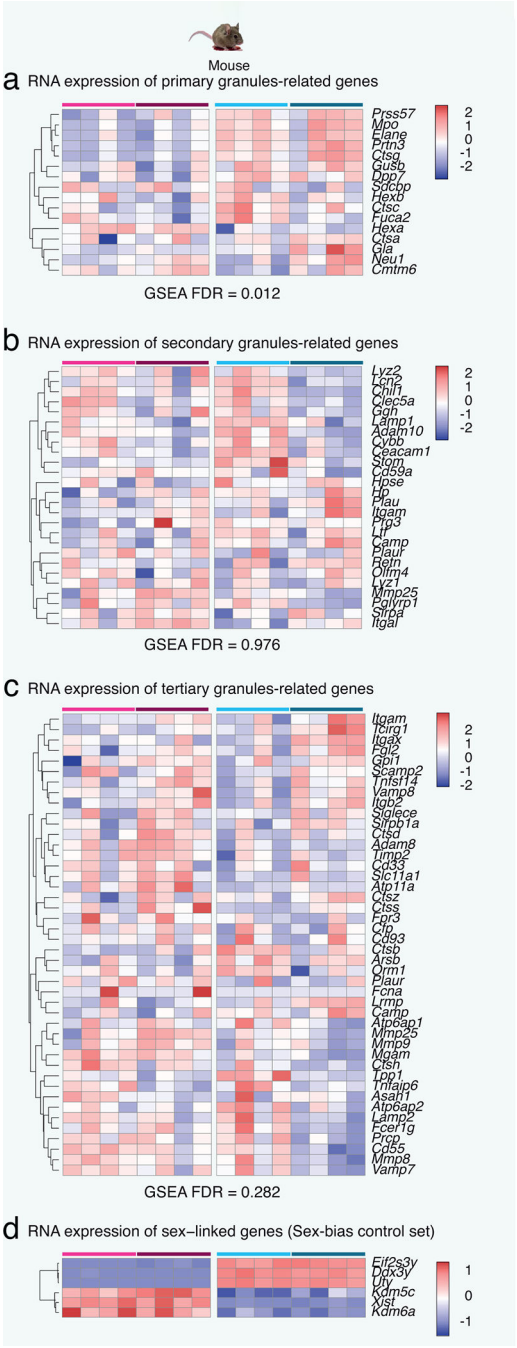

Extended Data Figure 10: Male neutrophils express higher levels of primary granule genes but not secondary and tertiary granule genes.

(**a-c**) Heatmap of normalized gene expression for primary (a), secondary (b) and tertiary (c) granule-related gene expression in our RNA-seq dataset. The estimated False Discovery Rate [FDR] using GSEA for each gene set is reported. (**d**) Heatmap of normalized gene expression for X-linked (*Kdm5c*, *Kdm6a*, *Xist*) and Y-linked (*Uty*, *Ddx3y*, *Eif2s3y*) genes in our RNA-seq dataset. Panel (a) is identical to Figure 7a to help direct comparison between sex-bias expression patterns of different granule types as well as canonical sex-biased genes. (**e-h**) Scatterplots of protein levels of DDX3Y (as a proxy for likely of a sample being derived from a male donor), compared to protein levels for primary granule-related proteins ELANE (e), MPO (f), PRTN3 (g) and CTSG (h) in neutrophils from healthy human donors. Normalized data was obtained from the supplementary material of [117]. Estimates of Spearman Rank correlation (Rho) and significance of correlation are reported for each correlation on the scatterplot.

Supplementary Material

Refer to Web version on PubMed Central for supplementary material.

Acknowledgements

We would like to thank Dr. Daniel Campo and Suchi Patel at the USC genome core for assistance in NGS-library quality control on the Agilent Bioanalyzer platform; Dr. Fan Li at the SC2 Core at CHLA for help with sequencing of transcriptomic libraries on the Illumina NextSeq550; Erin Christensen from Miltenyi Biotec for help designing and optimizing the flow cytometry panel. We thank Dr. Todd Morgan and Gerald Navarette from the USC Leonard Davis School of Gerontology mouse phenotyping core for assistance with CBC analyses on the Hemavet 950FS. We acknowledge the use of the HPC resource at USC for computational analyses. We thank Dr. Changhan Lee (USC), Dr. Kelvin Yen (USC), Dr. Sean P. Curran (USC), Dr. Marc Vermulst (USC), Dr. Helen Goodridge (Cedars-Sinai Medical Center) and Dr. Elsa Bou Ghanem (University at Buffalo) for helpful insights and feedback on our study. Finally, we thank lab members Ari Adler, Chan Boriboun, Cassandra McGill, Emily K. Wang and for helpful discussions and feedback on the study. We apologize for any papers not cited.

This work was supported by a Diana Jacobs Kalman/AFAR Scholarships for Research in the Biology of Aging (to R.J.L.), GCRLE-2020 post-doctoral fellowship from the Global Consortium for Reproductive Longevity and Equality at the Buck Institute, made possible by the Bia-Echo Foundation, (to M.K.), NIA T32 AG052374 and NSF graduate research fellowship DGE-1842487 (to J.I.B.), and NIA R00 AG049934, Pew Biomedical Scholar award #00034120, an innovator grant from the Rose Hills foundation, and the Kathleen Gilmore Biology of Aging research award (to B.A.B). This work was also partially supported by NCI Cancer Center Support Grant P30 CA014089 through the use of shared resources. The authors acknowledge the Center for Advanced Research Computing [CARC] at the University of Southern California for providing computing resources that have contributed to the research results reported within this publication (URL: https://carc.usc.edu).

References

1. Nah EH, Kim S, Cho S & Cho HI Complete Blood Count Reference Intervals and Patterns of Changes Across Pediatric, Adult, and Geriatric Ages in Korea. Ann Lab Med 38, 503–511 (2018). [PubMed: 30027692]
2. Furze RC & Rankin SM Neutrophil mobilization and clearance in the bone marrow. Immunology 125, 281–288 (2008). [PubMed: 19128361]
3. Shah B, Burg N & Pillinger MH Chapter 11 - Neutrophils. In: Firestein GS, Budd RC, Gabriel SE, McInnes IB & O'Dell JR (eds). Kelley and Firestein's Textbook of Rheumatology (Tenth Edition). Elsevier, 2017, pp 169–188.e163.
4. Ballesteros Iet al.Co-option of Neutrophil Fates by Tissue Environments. Cell183, 1282–1297 e1218 (2020). [PubMed: 33098771]

5. Lahoz-Beneytez Jet al.Human neutrophil kinetics: modeling of stable isotope labeling data supports short blood neutrophil half-lives. Blood127, 3431–3438 (2016). [PubMed: 27136946]
6. Pillay Jet al.In vivo labeling with 2H2O reveals a human neutrophil lifespan of 5.4 days. Blood116, 625–627 (2010). [PubMed: 20410504]
7. Zhang Det al.Neutrophil ageing is regulated by the microbiome. Nature525, 528–532 (2015). [PubMed: 26374999]
8. Sollberger G, Tilley DO & Zychlinsky A Neutrophil Extracellular Traps: The Biology of Chromatin Externalization. Dev Cell 44, 542–553 (2018). [PubMed: 29533770]
9. Soehnlein O, Steffens S, Hidalgo A & Weber C Neutrophils as protagonists and targets in chronic inflammation. Nat Rev Immunol 17, 248–261 (2017). [PubMed: 28287106]
10. Franceschi C & Campisi J Chronic inflammation (inflammaging) and its potential contribution to age-associated diseases. J Gerontol A Biol Sci Med Sci 69 Suppl 1, S4–9 (2014). [PubMed: 24833586]
11. Lu RJ, Wang EK & Benayoun BA Functional genomics of inflamm-aging and immunosenescence. Briefings in Functional Genomics (2021).
12. Tseng CW & Liu GY Expanding roles of neutrophils in aging hosts. Current Opinion in Immunology 29, 43–48 (2014). [PubMed: 24776646]
13. Hazeldine Jet al.Impaired neutrophil extracellular trap formation: a novel defect in the innate immune system of aged individuals. Aging Cell13, 690–698 (2014). [PubMed: 24779584]
14. Tseng CWet al.Innate immune dysfunctions in aged mice facilitate the systemic dissemination of methicillin-resistant S. aureus. PLoS One7, e41454 (2012). [PubMed: 22844481]
15. Sapey Eet al.Phosphoinositide 3-kinase inhibition restores neutrophil accuracy in the elderly: toward targeted treatments for immunosenescence. Blood123, 239–248 (2014). [PubMed: 24191150]
16. Simmons SR, Bhalla M, Herring SE, Tchalla EYI & Bou Ghanem EN Older but not wiser: The age-driven changes in neutrophil responses during pulmonary infections. Infect Immun (2021).
17. McLaughlin ME, Kao R, Liener IE & Hoidal JR A quantitative in vitro assay of polymorphonuclear leukocyte migration through human amnion membrane utilizing 111in-oxine. J Immunol Methods 95, 89–98 (1986). [PubMed: 3097158]
18. Benayoun BAet al.Remodeling of epigenome and transcriptome landscapes with aging in mice reveals widespread induction of inflammatory responses. Genome Res29, 697–709 (2019). [PubMed: 30858345]
19. Lai RWet al.Multi-level remodeling of transcriptional landscapes in aging and longevity. BMB Rep52, 86–108 (2019). [PubMed: 30526773]
20. Klein SL & Flanagan KL Sex differences in immune responses. Nat Rev Immunol 16, 626–638 (2016). [PubMed: 27546235]
21. Marquez EJet al.Sexual-dimorphism in human immune system aging. Nat Commun11, 751 (2020). [PubMed: 32029736]
22. Gal-Oz STet al.ImmGen report: sexual dimorphism in the immune system transcriptome. Nat Commun10, 4295 (2019). [PubMed: 31541153]
23. Markman JLet al.Loss of testosterone impairs anti-tumor neutrophil function. Nat Commun11, 1613 (2020). [PubMed: 32235862]
24. Gupta Set al.Sex differences in neutrophil biology modulate response to type I interferons and immunometabolism. Proc Natl Acad Sci U S A117, 16481–16491 (2020). [PubMed: 32601182]
25. Frisch BJet al.Aged marrow macrophages expand platelet-biased hematopoietic stem cells via interleukin-1B. JCI Insight4 (2019).
26. Kolaczkowska EThe older the faster: aged neutrophils in inflammation. Blood128, 2280–2282 (2016). [PubMed: 28829751]
27. Adrover JM, Nicolas-Avila JA & Hidalgo A Aging: A Temporal Dimension for Neutrophils. Trends Immunol 37, 334–345 (2016). [PubMed: 27083489]
28. Chen Xet al.ATAC-see reveals the accessible genome by transposase-mediated imaging and sequencing. Nat Methods13, 1013–1020 (2016). [PubMed: 27749837]

29. Denholtz Met al.Upon microbial challenge, human neutrophils undergo rapid changes in nuclear architecture and chromatin folding to orchestrate an immediate inflammatory gene program. Genes Dev34, 149–165 (2020). [PubMed: 31919189]
30. Papayannopoulos VNeutrophil extracellular traps in immunity and disease. Nat Rev Immunol18, 134–147 (2018). [PubMed: 28990587]
31. Brinkmann Vet al.Neutrophil extracellular traps kill bacteria. Science303, 1532–1535 (2004). [PubMed: 15001782]
32. Papayannopoulos V, Metzler KD, Hakkim A & Zychlinsky A Neutrophil elastase and myeloperoxidase regulate the formation of neutrophil extracellular traps. J Cell Biol 191, 677–691 (2010). [PubMed: 20974816]
33. Amulic Bet al.Cell-Cycle Proteins Control Production of Neutrophil Extracellular Traps. Developmental Cell43, 449–462.e445 (2017). [PubMed: 29103955]
34. Lopez-Otin C, Blasco MA, Partridge L, Serrano M & Kroemer G The hallmarks of aging. Cell 153, 1194–1217 (2013). [PubMed: 23746838]
35. Riffelmacher Tet al.Autophagy-Dependent Generation of Free Fatty Acids Is Critical for Normal Neutrophil Differentiation. Immunity47, 466–480 e465 (2017). [PubMed: 28916263]
36. Park SYet al.Autophagy Primes Neutrophils for Neutrophil Extracellular Trap Formation during Sepsis. Am J Respir Crit Care Med196, 577–589 (2017). [PubMed: 28358992]
37. Bhattacharya Aet al.Autophagy Is Required for Neutrophil-Mediated Inflammation. Cell Reports12, 1731–1739 (2015). [PubMed: 26344765]
38. Mitxelena Jet al.An E2F7-dependent transcriptional program modulates DNA damage repair and genomic stability. Nucleic acids research46, 4546–4559 (2018). [PubMed: 29590434]
39. Yuan Ret al.Cyclin F-dependent degradation of E2F7 is critical for DNA repair and G2-phase progression. The EMBO Journal38, e101430 (2019). [PubMed: 31475738]
40. Kim M-Het al.A late-lineage murine neutrophil precursor population exhibits dynamic changes during demand-adapted granulopoiesis. Scientific reports7, 39804–39804 (2017). [PubMed: 28059162]
41. Brown AK & Webb AE Regulation of FOXO Factors in Mammalian Cells. Curr Top Dev Biol 127, 165–192 (2018). [PubMed: 29433737]
42. Dong Get al.FOXO1 Regulates Bacteria-Induced Neutrophil Activity. Front Immunol8, 1088 (2017). [PubMed: 28928749]
43. Thiam HRet al.NETosis proceeds by cytoskeleton and endomembrane disassembly and PAD4-mediated chromatin decondensation and nuclear envelope rupture. Proceedings of the National Academy of Sciences117, 7326 (2020).
44. Rohrbach AS, Slade DJ, Thompson PR & Mowen KA Activation of PAD4 in NET formation. Front Immunol 3, 360–360 (2012). [PubMed: 23264775]
45. Cuthbert GLet al.Histone deimination antagonizes arginine methylation. Cell118, 545–553 (2004). [PubMed: 15339660]
46. Li Pet al.Regulation of p53 Target Gene Expression by Peptidylarginine Deiminase 4. Molecular and Cellular Biology28, 4745 (2008). [PubMed: 18505818]
47. Denis Het al.Functional connection between deimination and deacetylation of histones. Mol Cell Biol29, 4982–4993 (2009). [PubMed: 19581286]
48. Christophorou MAet al.Citrullination regulates pluripotency and histone H1 binding to chromatin. Nature507, 104–108 (2014). [PubMed: 24463520]
49. Hossain D, Barbelanne M & Tsang WY Requirement of NPHP5 in the hierarchical assembly of basal feet associated with basal bodies of primary cilia. Cell Mol Life Sci 77, 195–212 (2020). [PubMed: 31177295]
50. Marquis JFet al.Interferon regulatory factor 8 regulates pathways for antigen presentation in myeloid cells and during tuberculosis. PLoS Genet7, e1002097 (2011). [PubMed: 21731497]
51. Yáñez A, Ng MY, Hassanzadeh-Kiabi N & Goodridge HS IRF8 acts in lineage-committed rather than oligopotent progenitors to control neutrophil vs monocyte production. Blood 125, 1452–1459 (2015). [PubMed: 25597637]

52. Salem S, Salem D & Gros P Role of IRF8 in immune cells functions, protection against infections, and susceptibility to inflammatory diseases. Hum Genet 139, 707–721 (2020). [PubMed: 32232558]
53. Wynn TACellular and molecular mechanisms of fibrosis. J Pathol214, 199–210 (2008). [PubMed: 18161745]
54. Gregory ADet al.Neutrophil elastase promotes myofibroblast differentiation in lung fibrosis. J Leukoc Biol98, 143–152 (2015). [PubMed: 25743626]
55. Muller WATransendothelial migration: unifying principles from the endothelial perspective. Immunol Rev273, 61–75 (2016). [PubMed: 27558328]
56. Oh IH & Reddy EP The myb gene family in cell growth, differentiation and apoptosis. Oncogene 18, 3017–3033 (1999). [PubMed: 10378697]
57. Penniman CMet al.Loss of FoxOs in muscle reveals sex-based differences in insulin sensitivity but mitigates diet-induced obesity. Mol Metab30, 203–220 (2019). [PubMed: 31767172]
58. Austad SN & Bartke A Sex Differences in Longevity and in Responses to Anti-Aging Interventions: A Mini-Review. Gerontology 62, 40–46 (2015). [PubMed: 25968226]
59. Baker MJ, Pan D & Welch HC Small GTPases and their guanine-nucleotide exchange factors and GTPase-activating proteins in neutrophil recruitment. Curr Opin Hematol 23, 44–54 (2016). [PubMed: 26619317]
60. Richer BC, Salei N, Laskay T & Seeger K Changes in Neutrophil Metabolism upon Activation and Aging. Inflammation 41, 710–721 (2018). [PubMed: 29322364]
61. Eltzschig HKet al.Endogenous adenosine produced during hypoxia attenuates neutrophil accumulation: coordination by extracellular nucleotide metabolism. Blood104, 3986–3992 (2004). [PubMed: 15319286]
62. Eltzschig HKet al.ATP release from activated neutrophils occurs via connexin 43 and modulates adenosine-dependent endothelial cell function. Circ Res99, 1100–1108 (2006). [PubMed: 17038639]
63. Mondanelli G, Iacono A, Allegrucci M, Puccetti P & Grohmann U Immunoregulatory Interplay Between Arginine and Tryptophan Metabolism in Health and Disease. Front Immunol 10, 1565 (2019). [PubMed: 31354721]
64. Jarc E & Petan T A twist of FATe: Lipid droplets and inflammatory lipid mediators. Biochimie 169, 69–87 (2020). [PubMed: 31786231]
65. Schlager Set al.Adipose triglyceride lipase acts on neutrophil lipid droplets to regulate substrate availability for lipid mediator synthesis. J Leukoc Biol98, 837–850 (2015). [PubMed: 26109679]
66. Meana Cet al.Lipin-1 Integrates Lipid Synthesis with Proinflammatory Responses during TLR Activation in Macrophages. The Journal of Immunology193, 4614 (2014). [PubMed: 25252959]
67. Buenrostro JD, Giresi PG, Zaba LC, Chang HY & Greenleaf WJ Transposition of native chromatin for fast and sensitive epigenomic profiling of open chromatin, DNA-binding proteins and nucleosome position. Nat Methods 10, 1213–1218 (2013). [PubMed: 24097267]
68. Schep ANet al.Structured nucleosome fingerprints enable high-resolution mapping of chromatin architecture within regulatory regions. Genome Res25, 1757–1770 (2015). [PubMed: 26314830]
69. Janssen A, Colmenares SU & Karpen GH Heterochromatin: Guardian of the Genome. Annu Rev Cell Dev Biol 34, 265–288 (2018). [PubMed: 30044650]
70. Neubert Eet al.Chromatin swelling drives neutrophil extracellular trap release. Nature Communications9, 3767 (2018).
71. Itou T, Collins LV, Thoren FB, Dahlgren C & Karlsson A Changes in activation states of murine polymorphonuclear leukocytes (PMN) during inflammation: a comparison of bone marrow and peritoneal exudate PMN. Clin Vaccine Immunol 13, 575–583 (2006). [PubMed: 16682479]
72. Consortium EPAn integrated encyclopedia of DNA elements in the human genome. Nature489, 57–74 (2012). [PubMed: 22955616]
73. Rausch C, Hastert FD & Cardoso MC DNA Modification Readers and Writers and Their Interplay. Journal of Molecular Biology 432, 1731–1746 (2020).
74. Horvath S & Raj K DNA methylation-based biomarkers and the epigenetic clock theory of ageing. Nat Rev Genet 19, 371–384 (2018). [PubMed: 29643443]

75. Feldman GMet al.STAT5A-deficient mice demonstrate a defect in granulocyte-macrophage colony-stimulating factor-induced proliferation and gene expression. Blood90, 1768–1776 (1997). [PubMed: 9292509]
76. Kimura Aet al.The transcription factors STAT5A/B regulate GM-CSF-mediated granulopoiesis. Blood114, 4721–4728 (2009). [PubMed: 19779039]
77. Zhang Zet al.PRC2 complexes with JARID2, MTF2, and esPRC2p48 in ES cells to modulate ES cell pluripotency and somatic cell reprogramming. Stem Cells29, 229–240 (2011). [PubMed: 21732481]
78. Perino Met al.MTF2 recruits Polycomb Repressive Complex 2 by helical-shape-selective DNA binding. Nat Genet50, 1002–1010 (2018). [PubMed: 29808031]
79. Girardin SEet al.Nod2 is a general sensor of peptidoglycan through muramyl dipeptide (MDP) detection. J Biol Chem278, 8869–8872 (2003). [PubMed: 12527755]
80. Billmann-Born Set al.Genome-Wide Expression Profiling Identifies an Impairment of Negative Feedback Signals in the Crohn's Disease-Associated NOD2 Variant L1007fsinsC. The Journal of Immunology186, 4027 (2011). [PubMed: 21335489]
81. Jeong YJet al.Nod2 and Rip2 contribute to innate immune responses in mouse neutrophils. Immunology143, 269–276 (2014). [PubMed: 24766550]
82. Kanfi Yet al.The sirtuin SIRT6 regulates lifespan in male mice. Nature483, 218–221 (2012). [PubMed: 22367546]
83. Peshti Vet al.Characterization of physiological defects in adult SIRT6−/− mice. PloS one12, e0176371–e0176371 (2017). [PubMed: 28448551]
84. Kawahara TLet al.SIRT6 links histone H3 lysine 9 deacetylation to NF-kappaB-dependent gene expression and organismal life span. Cell136, 62–74 (2009). [PubMed: 19135889]
85. Lappas MAnti-inflammatory properties of sirtuin 6 in human umbilical vein endothelial cells. Mediators Inflamm2012, 597514 (2012). [PubMed: 23132960]
86. Xiao Cet al.Progression of chronic liver inflammation and fibrosis driven by activation of c-JUN signaling in Sirt6 mutant mice. J Biol Chem287, 41903–41913 (2012). [PubMed: 23076146]
87. Chen Xet al.The Forkhead Transcription Factor FOXM1 Controls Cell Cycle-Dependent Gene Expression through an Atypical Chromatin Binding Mechanism. Molecular and Cellular Biology33, 227 (2013). [PubMed: 23109430]
88. Zhan Met al.The B-MYB transcriptional network guides cell cycle progression and fate decisions to sustain self-renewal and the identity of pluripotent stem cells. PLoS One7, e42350 (2012). [PubMed: 22936984]
89. Baker SJet al.B-myb is an essential regulator of hematopoietic stem cell and myeloid progenitor cell development. Proc Natl Acad Sci U S A111, 3122–3127 (2014). [PubMed: 24516162]
90. Jung SMet al.Non-canonical mTORC2 Signaling Regulates Brown Adipocyte Lipid Catabolism through SIRT6-FoxO1. Mol Cell75, 807–822 e808 (2019). [PubMed: 31442424]
91. He Jet al.SIRT6 reduces macrophage foam cell formation by inducing autophagy and cholesterol efflux under ox-LDL condition. FEBS J284, 1324–1337 (2017). [PubMed: 28296196]
92. Feldman JL, Baeza J & Denu JM Activation of the protein deacetylase SIRT6 by long-chain fatty acids and widespread deacylation by mammalian sirtuins. J Biol Chem 288, 31350–31356 (2013). [PubMed: 24052263]
93. Lacy PMechanisms of degranulation in neutrophils. Allergy Asthma Clin Immunol2, 98–108 (2006). [PubMed: 20525154]
94. Belaaouaj Aet al.Mice lacking neutrophil elastase reveal impaired host defense against gram negative bacterial sepsis. Nat Med4, 615–618 (1998). [PubMed: 9585238]
95. Okeke EBet al.Inhibition of neutrophil elastase prevents neutrophil extracellular trap formation and rescues mice from endotoxic shock. Biomaterials238, 119836 (2020). [PubMed: 32045782]
96. Raduolovic K, Mak'Anyengo R, Kaya B, Steinert A & Niess JH Injections of Lipopolysaccharide into Mice to Mimic Entrance of Microbial-derived Products After Intestinal Barrier Breach. J Vis Exp (2018).

97. Grabowski Pet al.Proteome Analysis of Human Neutrophil Granulocytes From Patients With Monogenic Disease Using Data-independent Acquisition. Molecular & Cellular Proteomics18, 760 (2019). [PubMed: 30630937]

98. Chua F & Laurent GJ Neutrophil elastase: mediator of extracellular matrix destruction and accumulation. Proc Am Thorac Soc 3, 424–427 (2006). [PubMed: 16799086]

99. Sampathkumar NKet al.Widespread sex dimorphism in aging and age-related diseases. Hum Genet139, 333–356 (2020). [PubMed: 31677133]

100. Kovats SEstrogen receptors regulate innate immune cells and signaling pathways. Cell Immunol294, 63–69 (2015). [PubMed: 25682174]

101. Angele MK, Pratschke S, Hubbard WJ & Chaudry IH Gender differences in sepsis: cardiovascular and immunological aspects. Virulence 5, 12–19 (2014). [PubMed: 24193307]

102. Scully EP, Haverfield J, Ursin RL, Tannenbaum C & Klein SL Considering how biological sex impacts immune responses and COVID-19 outcomes. Nature Reviews Immunology (2020).

103. Barnes BJet al.Targeting potential drivers of COVID-19: Neutrophil extracellular traps. J Exp Med217 (2020).

104. Ghosh Set al.Neutrophils homing into the retina trigger pathology in early age-related macular degeneration. Commun Biol2, 348 (2019). [PubMed: 31552301]

105. Roy-O'Reilly MAet al.Aging exacerbates neutrophil pathogenicity in ischemic stroke. Aging (Albany NY)12, 436–461 (2020). [PubMed: 31927534]

106. Meijer M, Rijkers GT & van Overveld FJ Neutrophils and emerging targets for treatment in chronic obstructive pulmonary disease. Expert Rev Clin Immunol 9, 1055–1068 (2013). [PubMed: 24168412]

107. Ionita MGet al.High neutrophil numbers in human carotid atherosclerotic plaques are associated with characteristics of rupture-prone lesions. Arterioscler Thromb Vasc Biol30, 1842–1848 (2010). [PubMed: 20595650]

108. Treffers LW, Hiemstra IH, Kuijpers TW, van den Berg TK & Matlung HL Neutrophils in cancer. Immunol Rev 273, 312–328 (2016). [PubMed: 27558343]

109. Breuer Ket al.InnateDB: systems biology of innate immunity and beyond--recent updates and continuing curation. Nucleic Acids Res41, D1228–1233 (2013). [PubMed: 23180781]

110. Amend SR, Valkenburg KC & Pienta KJ Murine Hind Limb Long Bone Dissection and Bone Marrow Isolation. JoVE, e53936 (2016).

111. Kwok Iet al.Combinatorial Single-Cell Analyses of Granulocyte-Monocyte Progenitor Heterogeneity Reveals an Early Uni-potent Neutrophil Progenitor. Immunity53, 303–318 e305 (2020). [PubMed: 32579887]

112. Evrard Met al.Developmental Analysis of Bone Marrow Neutrophils Reveals Populations Specialized in Expansion, Trafficking, and Effector Functions. Immunity48, 364–379 e368 (2018). [PubMed: 29466759]

113. Adrover JMet al.A Neutrophil Timer Coordinates Immune Defense and Vascular Protection. Immunity50, 390–402 e310 (2019). [PubMed: 30709741]

114. Dobin Aet al.STAR: ultrafast universal RNA-seq aligner. Bioinformatics29, 15–21 (2013). [PubMed: 23104886]

115. Liao Y, Smyth GK & Shi W featureCounts: an efficient general purpose program for assigning sequence reads to genomic features. Bioinformatics 30, 923–930 (2014). [PubMed: 24227677]

116. Leek JT & Storey JD Capturing heterogeneity in gene expression studies by surrogate variable analysis. PLoS Genet 3, 1724–1735 (2007). [PubMed: 17907809]

117. Love MI, Huber W & Anders S Moderated estimation of fold change and dispersion for RNA-seq data with DESeq2. Genome Biology 15, 550 (2014). [PubMed: 25516281]

118. Chen Y & Meltzer PS Gene expression analysis via multidimensional scaling. Curr Protoc Bioinformatics Chapter 7, Unit 7 11 (2005).

119. Zhou Get al.NetworkAnalyst 3.0: a visual analytics platform for comprehensive gene expression profiling and meta-analysis. Nucleic Acids Res47, W234–W241 (2019). [PubMed: 30931480]

120. Subramanian Aet al.Gene set enrichment analysis: A knowledge-based approach for interpreting genome-wide expression profiles. Proceedings of the National Academy of Sciences102, 15545 (2005).

121. Liberzon Aet al.Molecular signatures database (MSigDB) 3.0. Bioinformatics27, 1739–1740 (2011). [PubMed: 21546393]

122. Rouillard ADet al.The harmonizome: a collection of processed datasets gathered to serve and mine knowledge about genes and proteins. Database (Oxford)2016 (2016).

123. Contrepois Ket al.Cross-Platform Comparison of Untargeted and Targeted Lipidomics Approaches on Aging Mouse Plasma. Sci Rep8, 17747 (2018). [PubMed: 30532037]

124. Contrepois K, Jiang L & Snyder M Optimized Analytical Procedures for the Untargeted Metabolomic Profiling of Human Urine and Plasma by Combining Hydrophilic Interaction (HILIC) and Reverse-Phase Liquid Chromatography (RPLC)-Mass Spectrometry. Mol Cell Proteomics 14, 1684–1695 (2015). [PubMed: 25787789]

125. Tyanova Set al.The Perseus computational platform for comprehensive analysis of (prote)omics data. Nat Methods13, 731–740 (2016). [PubMed: 27348712]

126. Shen Xet al.Metabolic reaction network-based recursive metabolite annotation for untargeted metabolomics. Nat Commun10, 1516 (2019). [PubMed: 30944337]

127. Jauhiainen Aet al.Normalization of metabolomics data with applications to correlation maps. Bioinformatics30, 2155–2161 (2014). [PubMed: 24711654]

128. Li Bet al.Performance Evaluation and Online Realization of Data-driven Normalization Methods Used in LC/MS based Untargeted Metabolomics Analysis. Scientific Reports6, 38881 (2016). [PubMed: 27958387]

129. Chong J & Xia J MetaboAnalystR: an R package for flexible and reproducible analysis of metabolomics data. Bioinformatics 34, 4313–4314 (2018). [PubMed: 29955821]

130. Ried JSet al.PSEA: Phenotype Set Enrichment Analysis--a new method for analysis of multiple phenotypes. Genet Epidemiol36, 244–252 (2012). [PubMed: 22714936]

131. Li Set al.Predicting Network Activity from High Throughput Metabolomics. PLOS Computational Biology9, e1003123 (2013). [PubMed: 23861661]

132. Kamburov A, Cavill R, Ebbels TMD, Herwig R & Keun HC Integrated pathway-level analysis of transcriptomics and metabolomics data with IMPaLA. Bioinformatics 27, 2917–2918 (2011). [PubMed: 21893519]

133. Molenaar MRet al.LION/web: a web-based ontology enrichment tool for lipidomic data analysis. Gigascience8 (2019).

134. Corces MRet al.An improved ATAC-seq protocol reduces background and enables interrogation of frozen tissues. Nat Methods14, 959–962 (2017). [PubMed: 28846090]

135. Gaspar JMNGmerge: merging paired-end reads via novel empirically-derived models of sequencing errors. BMC Bioinformatics19, 536 (2018). [PubMed: 30572828]

136. Langmead B & Salzberg SL Fast gapped-read alignment with Bowtie 2. Nat Methods 9, 357–359 (2012). [PubMed: 22388286]

137. Heinz Set al.Simple combinations of lineage-determining transcription factors prime cis-regulatory elements required for macrophage and B cell identities. Mol Cell38, 576–589 (2010). [PubMed: 20513432]

138. Ross-Innes CSet al.Differential oestrogen receptor binding is associated with clinical outcome in breast cancer. Nature481, 389–393 (2012). [PubMed: 22217937]

139. McLean CYet al.GREAT improves functional interpretation of cis-regulatory regions. Nat Biotechnol28, 495–501 (2010). [PubMed: 20436461]

140. King HW, Fursova NA, Blackledge NP & Klose RJ Polycomb repressive complex 1 shapes the nucleosome landscape but not accessibility at target genes. Genome Res 28, 1494–1507 (2018). [PubMed: 30154222]

141. Masuda Set al.Measurement of NET formation in vitro and in vivo by flow cytometry. Cytometry A91, 822–829 (2017). [PubMed: 28715618]

142. Carmona-Rivera C & Kaplan MJ Induction and Quantification of NETosis. Curr Protoc Immunol 115, 14 41 11–14 41 14 (2016).

143. Goh WWB, Wang W & Wong L Why Batch Effects Matter in Omics Data, and How to Avoid Them. Trends Biotechnol 35, 498–507 (2017). [PubMed: 28351613]

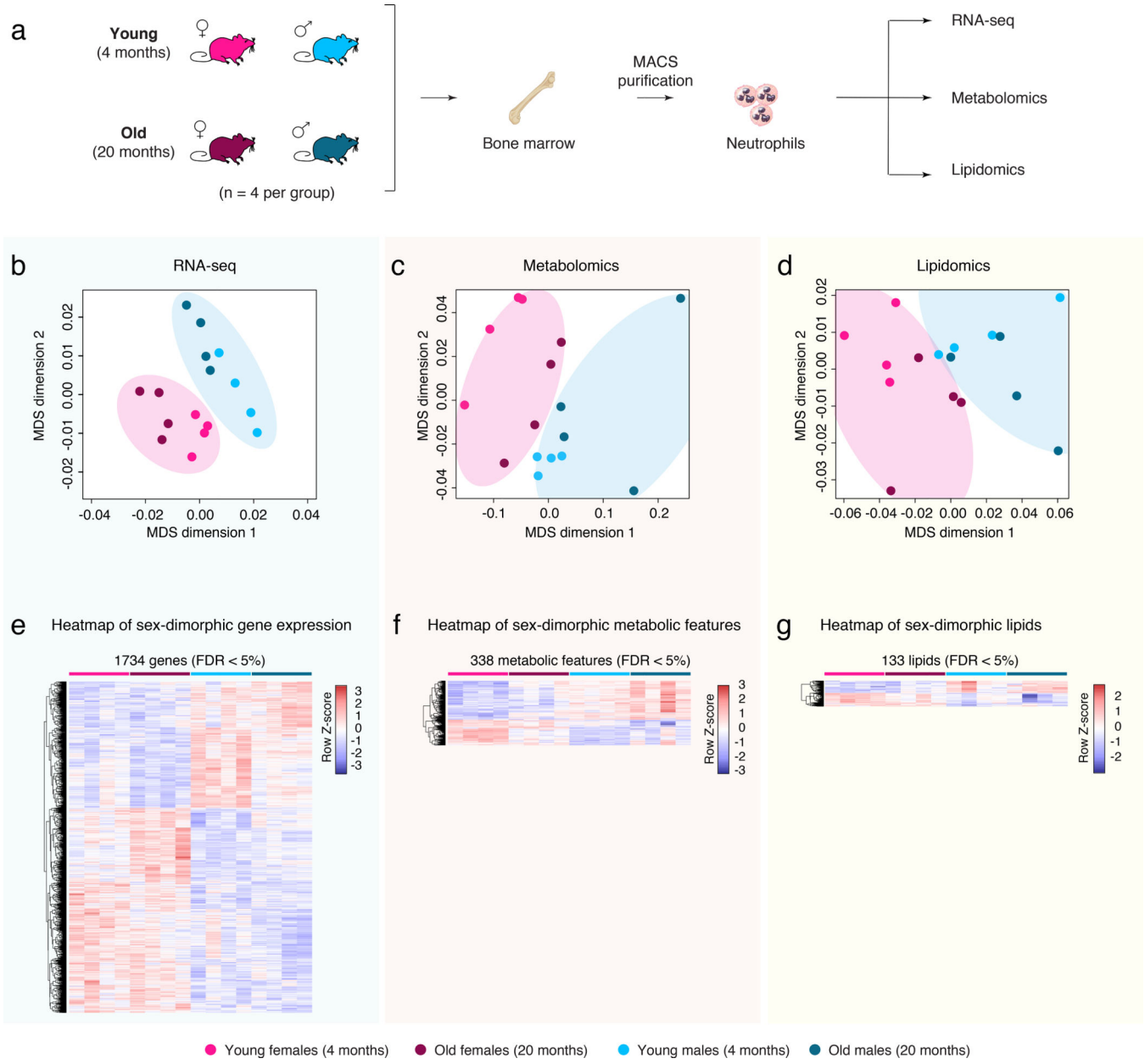

Figure 1: A multi-omic analysis of primary mouse bone marrow neutrophils during aging and with respect to sex.

(**a**) Experimental setup scheme. (**b-d**) Multidimensional Scaling analysis results of RNA expression by RNA-seq (b), untargeted metabolomics (c), or targeted lipidomics (d). (**e-g**) Heatmap of significant (FDR < 5%) sex-dimorphic genes (e), metabolic features (f) or lipid species (g). Significance of gene regulation by RNA-seq was calculated by DESeq2, and significance of metabolic features or lipid species regulation were calculated by limma. MACS: Magnetic-Activated Cell Sorting. MDS: Multidimensional Scaling.

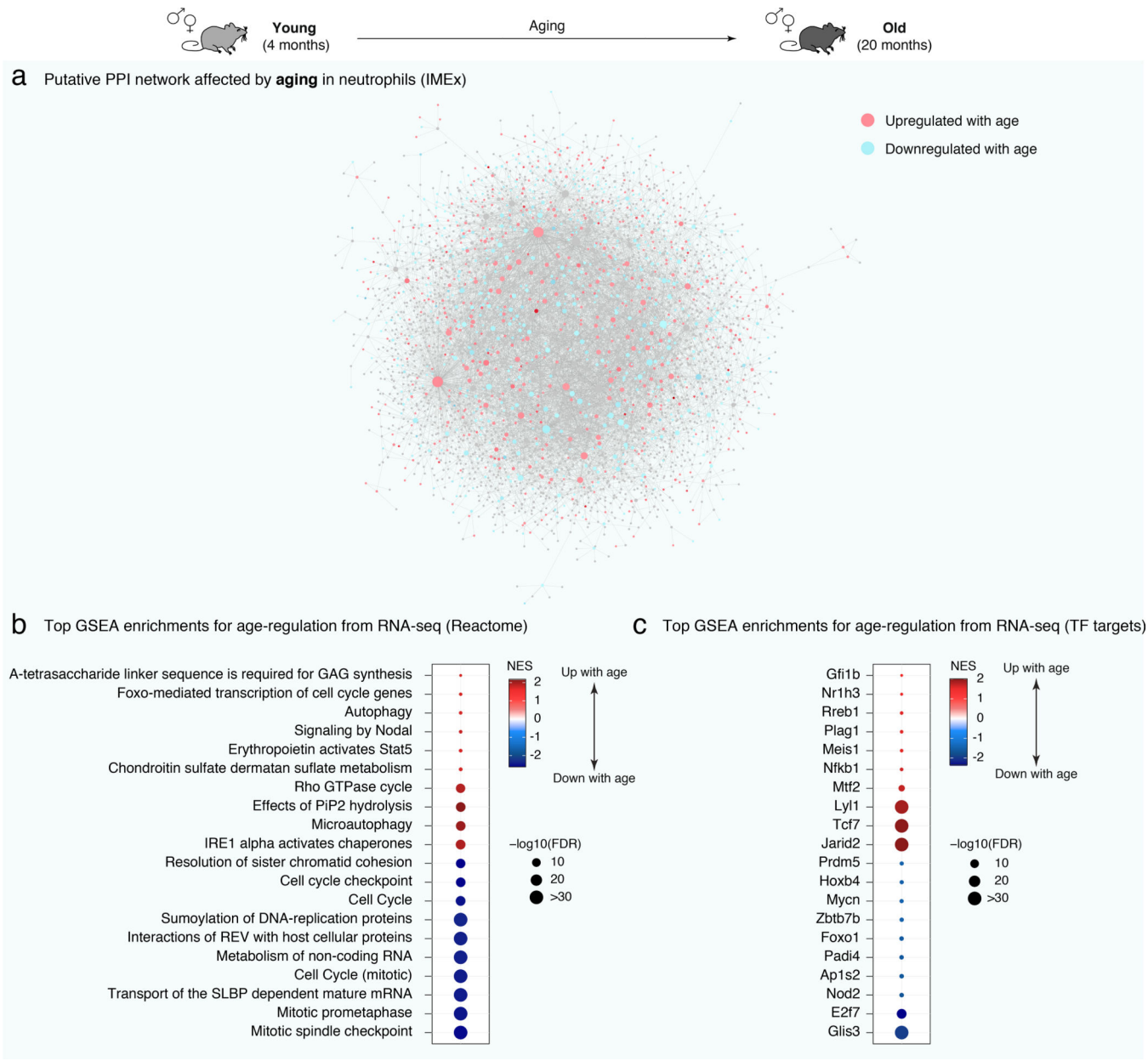

Figure 2: Regulated pathways in bone marrow neutrophils during aging reveals downregulation of chromatin-related pathways.

(**a**) NetworkAnalyst predicted PPI network for significant age-regulated genes in neutrophils. Network edges are based on IMEx/InnateDB data, a knowledgebase specifically geared for analyses of innate immune networks [109]. Blue (red) shades are associated to decreased (increased) gene expression during aging. (**b-c**) Top enriched gene sets from Reactome (b) and transcription factor targets (c) using GSEA for differential RNA expression. Only the top 10 most up- and top 10 most downregulated gene sets are plotted for readability. Full lists and statistics available in Supplementary Table S3. Also see Extended Data Figure 5. Shown pathways with FDR < 5%. NES: Normalized Enrichment Score (for GSEA analysis). FDR: False Discovery Rate.

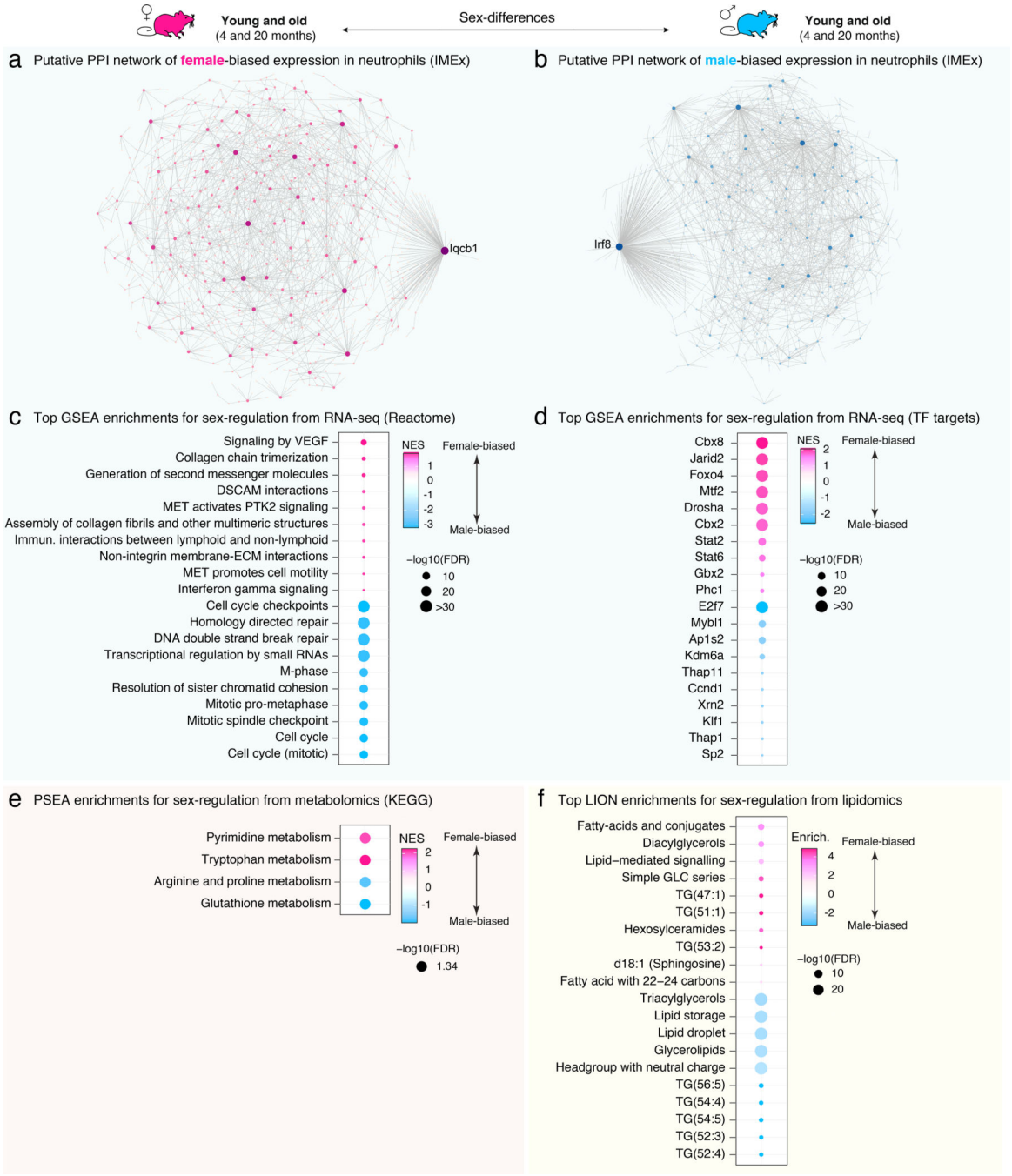

Figure 3: Sex-dimorphic pathways in bone marrow neutrophils reveal differential regulation of chromatin-related pathways.

(**a-b**) NetworkAnalyst predicted PPI networks for genes displaying significant bias in gene expression by RNA-seq towards female (a) or male (b) neutrophils. Network edges are based on IMEx/InnateDB data, a knowledgebase specifically geared for analyses of innate immune networks [109]. (**c-d**) Top enriched gene sets from Reactome (c) and transcription factor targets (d) using GSEA for differential RNA expression. (**e**) Phenotype Set Enrichment Analysis (PSEA) for differential metabolite regulation. (**f**) Top Lipid Ontology (LION)

functional enrichment analysis for differential lipid regulation. For (c-f), the top 10 most up- and top 10 most downregulated gene sets (if that many) are plotted for readability. Full lists and statistics available in Supplementary Table S4. Also see Extended Data Figure 7. Shown pathways with FDR < 5%. NES: Normalized Enrichment Score (for GSEA and PSEA analysis). FDR: False Discovery Rate.

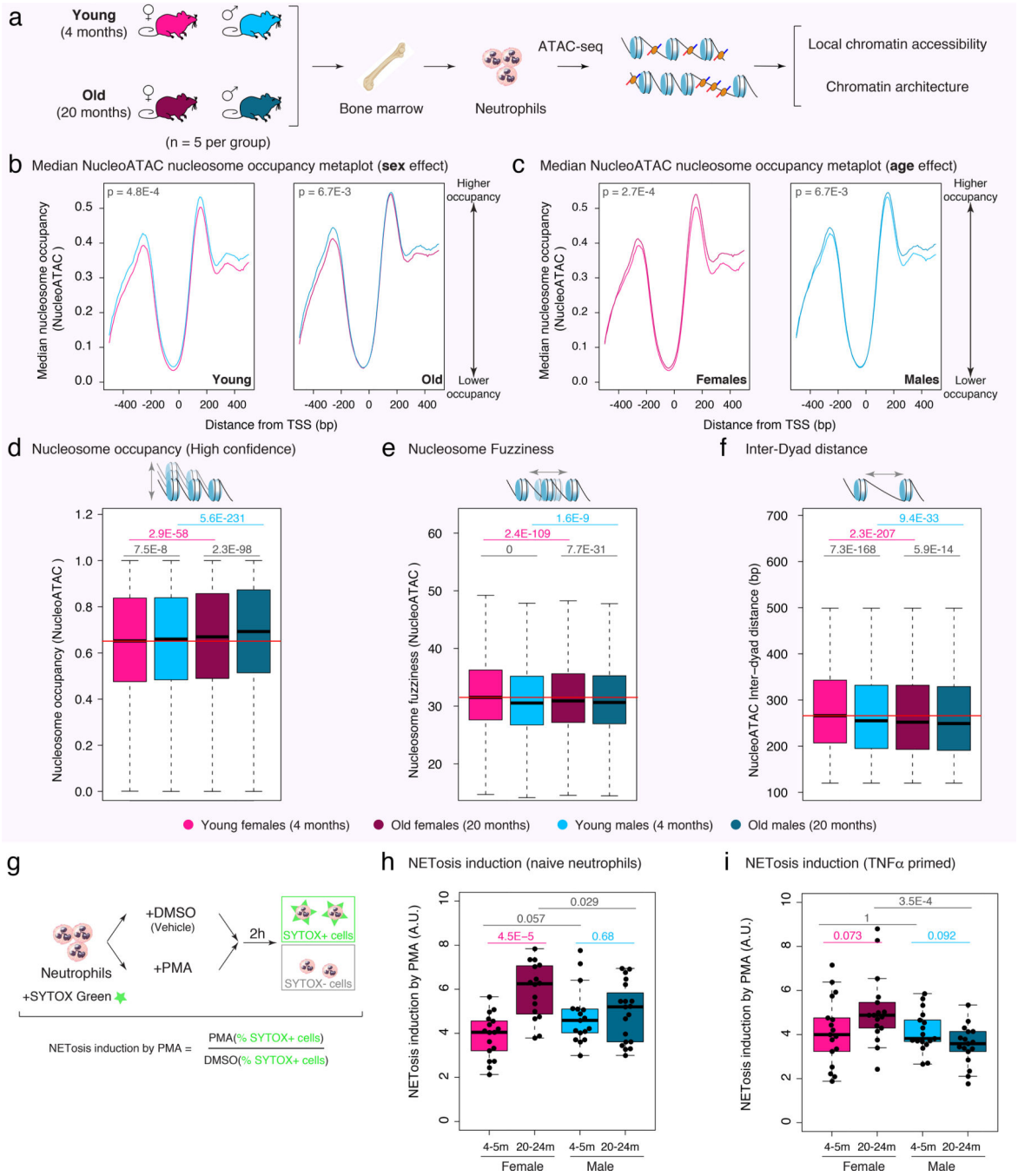

Figure 4: ATAC-seq analysis reveals age- and sex-related differences in the chromatin architecture of bone marrow neutrophils.

(**a**) Setup scheme for ATAC-seq experiment. (**b-c**) Metaplot analysis of median nucleosome occupancy (as calculated by NucleoATAC) around the TSS of neutrophil-expressed genes, to analyze sex- (b) or age-related (c) differences in neutrophil nucleosome occupancy. Note that increased occupancy is observed in male compared to female neutrophils, as well as in old compared to young neutrophils. Significance of the difference between median occupancy profiles at TSSs assessed using a two-sided Kolmogorov-Smirnov goodness-of-

fit test for (b,c). (**d**) Boxplot of nucleosome occupancy as calculated by NucleoATAC for high-confidence nucleosomes across groups. Also see Extended Data Figure 8i. (**e**) Boxplot of nucleosome fuzziness as calculated by NucleoATAC for high-confidence nucleosomes across experimental groups. (**f**) Boxplot of nucleosome inter-dyad distance as calculated by NucleoATAC across experimental groups. The horizontal red line in panels (**d-f**) shows the median value in neutrophils from young females for ease of comparison. Significance in non-parametric two-sided Wilcoxon rank-sum tests is reported for panels (**d-f**). Black p-values represent differences between male *vs.* female neutrophils in each age group; pink (blue) p-values represent age-related differences in female (male) neutrophils. Also see Extended Data Figure 8i,j. (**g**) Workflow for the *in vitro* NETosis inducibility experiment. SYTOX Green was used to stain extracellular DNA, a proxy for NETosing cells. (**h**) Boxplot of NETosis induction in naïve neutrophils. Each point represents one animal, median of 4 technical replicates. Animals from 4 independent cohorts, n = 16–19 per group (variation due to animal death prior to experiment and technical failures of the flow cytometer on some samples; n = 17 for young males and females; n = 16 for old females; n = 19 for old males). (**i**) Boxplot of NETosis induction in neutrophils, primed with 10ng/mL mouse TNFα for 10 min prior to NETosis induction. Each point represents one animal, median of 4 technical replicates. Animals from 4 independent cohorts, n = 17 per group. Significance in non-parametric two-sided Wilcoxon rank-sum tests are reported for panels (**h-i**). Black p-values represent differences between male *vs.* female neutrophils in each age group; pink (blue) p-values represent age-related differences in female (male) neutrophils. For all boxplots in panels (**d-f, h-i**), the center line represents the sample median, the box limits consist of the 25^{th} and 75^{th} percentiles, the whiskers span 1.5x the interquartile range. For (d-f), for readability and consistent with practices in genomics, outliers are not shown on the graph although they are always taken into account for the statistics.

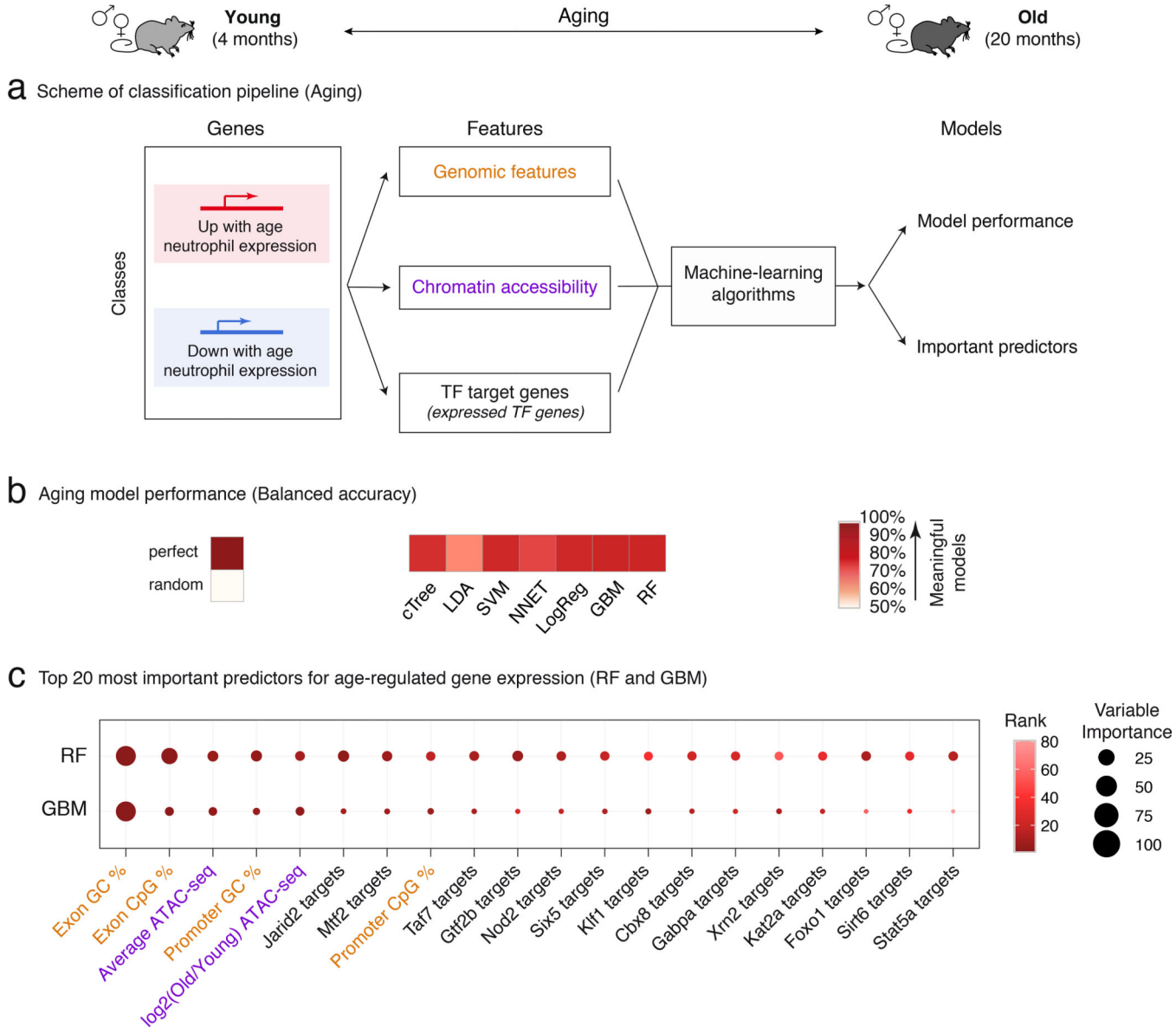

Figure 5: Machine-learning analysis reveals that age-regulated gene expression can be predicted by genomic and epigenomic features.

(**a**) Scheme of our machine-learning pipeline for up *vs.* downregulated genes in neutrophils with aging. (**b**) Balanced classification accuracy over different machine-learning model algorithms. The accuracy of the models is measured using held-out testing data. 'Random' accuracy illustrates the accuracy of a meaningless model (~50%), and 'perfect' that of a model with no mistakes (100%). All tests were more accurate than random (see other measures of model performance in Extended Data Figure 9a–c and Supplementary Table S5A). (**c**) Top 20 most important features from Random Forest models and Gradient Boosting Machine models. A rank product approach was used to determine overall top predictive features from both models. High values for variable importance indicate most influential predictors. cTree: conditional inference tree, LDA: linear discriminant analysis,

SVM: support vector machine, NNET: neural network, LogReg: logistic regression, GBM: gradient boosting machine, RF: random forest.

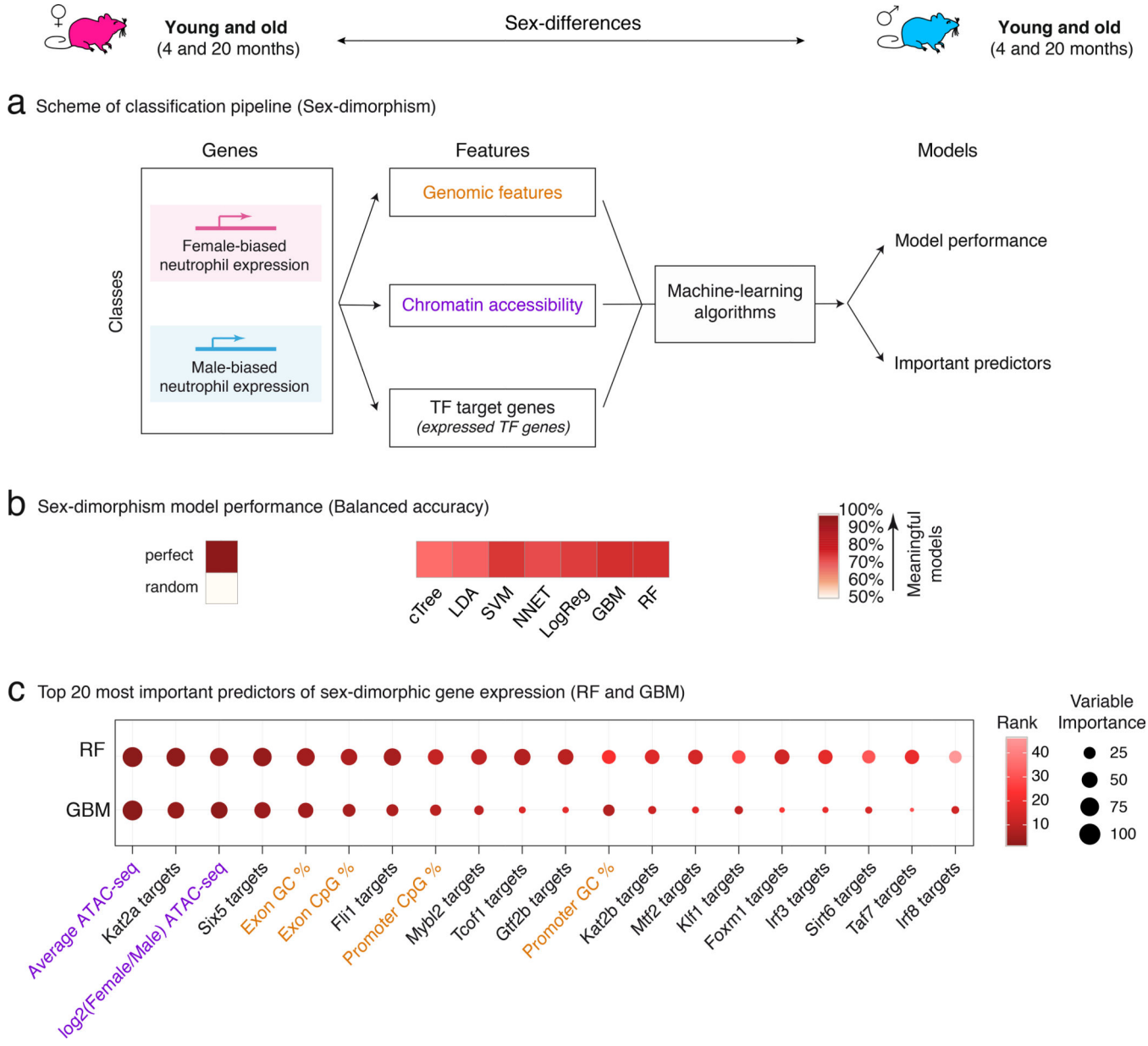

Figure 6: Machine-learning analysis reveals that sex-dimorphic gene expression can be predicted by genomic and epigenomic features.

(**a**) Scheme of our machine-learning pipeline for male *vs.* female-biased gene expression in neutrophils. (**b**) Balanced classification accuracy over different machine-learning model algorithms. The accuracy of the models is measured using held-out testing data. 'Random' accuracy illustrates the accuracy of a meaningless model (~50%), and 'perfect' that of a model with no mistakes (100%). All tests were more accurate than random (see other measures of model performance in Extended Data Figure 9d–f and Supplementary Table S5C). (**c**) Top 20 most important features from Random Forest models and Gradient Boosting Machine models. A rank product approach was used to determine overall top predictive features from both models. High values for variable importance indicate most influential predictors. cTree: conditional inference tree, LDA: linear discriminant analysis,

SVM: support vector machine, NNET: neural network, LogReg: logistic regression, GBM: gradient boosting machine, RF: random forest.

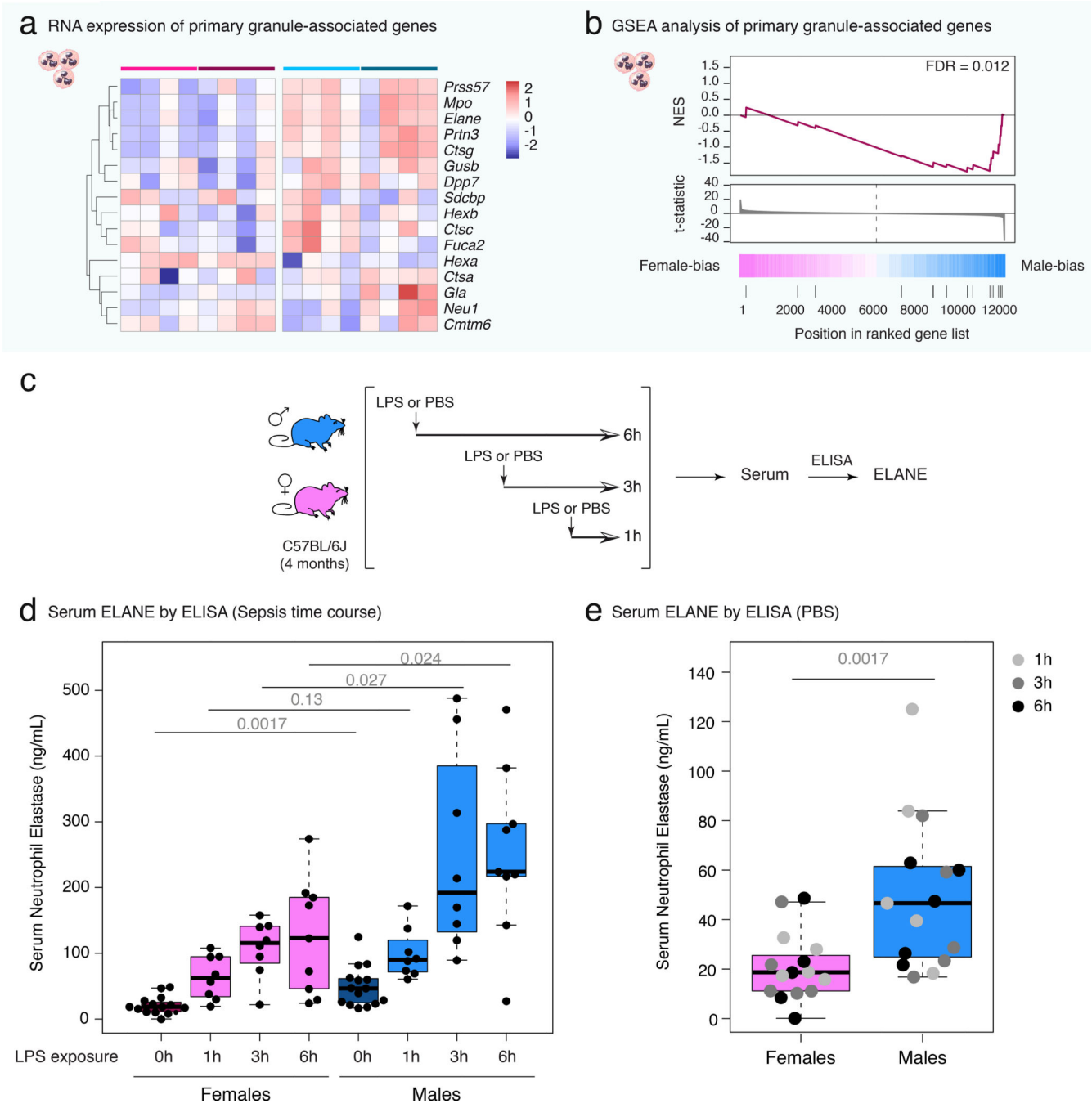

Figure 7: Male neutrophils express higher levels of primary granule genes, correlating with increased serum ELANE levels in control and septic mice.

(**a**) Heatmap of normalized gene expression for primary (azurophilic) granule-related gene expression in our RNA-seq dataset. Also see Extended Data Figure 10. (**b**) GSEA analysis of primary (azurophilic) granule-related gene expression reveals biased expression to male neutrophils. (**c**) Setup scheme for serum ELANE measurement in control and sepsis-like mice. (**d-e**) Analysis of ELANE protein levels in mouse serum by ELISA. The data is derived from 3 independent cohorts of young male *vs.* female mice (n = 5 per sex and time

point for 1, 3 and 6h PBS injection; n = 8 per sex and time point for 1 and 3h LPS, and n = 9 per sex and time point for 6h LPS injection). For simplicity's sake, all PBS-injected animals are reported as "0h of LPS exposure" in (d) and are replotted with time-based color-coding in (e). Significance in non-parametric two-sided Wilcoxon rank-sum test. For boxplots in panels (**d-e**), the center line represents the sample median, the box limits consist of the 25th and 75th percentiles, the whiskers span 1.5x the interquartile range.